Atmos. Chem. Phys., 20, 5355–5372, 2020
https://doi.org/10.5194/acp-20-5355-2020

Atmospheric Chemistry and Physics
Open Access
EGU

Exploring wintertime regional haze in northeast China: role of coal and biomass burning

Jian Zhang[1], Lei Liu[1], Liang Xu[1], Qiuhan Lin[1], Hujia Zhao[2], Zhibin Wang[3], Song Guo[4], Min Hu[4], Dantong Liu[1], Zongbo Shi[5], Dao Huang[1], and Weijun Li[1]

[1]Department of Atmospheric Sciences, School of Earth Sciences, Zhejiang University, Hangzhou, 310027, China
[2]Institute of Atmospheric Environment, China Meteorological Administration, Shenyang, 110016, China
[3]Research Center for Air Pollution and Health, College of Environmental and Resource Sciences, Zhejiang University, Hangzhou, 310058, China
[4]State Key Joint Laboratory of Environmental Simulation and Pollution Control, College of Environmental Sciences and Engineering, Peking University, Beijing, 100871, China
[5]School of Geography, Earth and Environmental Sciences, University of Birmingham, Birmingham, B15 2TT, UK

Correspondence: Weijun Li (liweijun@zju.edu.cn)

Received: 6 November 2019 – Discussion started: 8 January 2020
Revised: 18 March 2020 – Accepted: 1 April 2020 – Published: 7 May 2020

Abstract. As one of the intense anthropogenic emission regions across the relatively high-latitude ($> 40°$ N) areas on Earth, northeast China faces the serious problem of regional haze during the heating period of the year. Aerosols in polluted haze in northeast China are poorly understood compared with the haze in other regions of China such as the North China Plain. Here, we integrated bulk chemical measurements with single-particle analysis from transmission electron microscopy (TEM), nanoscale secondary ion mass spectrometry (NanoSIMS), and atomic force microscopy (AFM) to obtain morphology, size, composition, aging process, and sources of aerosol particles collected during two contrasting regional haze events (Haze-I and Haze-II) at an urban site and a mountain site in northeast China and further investigated the causes of regional haze formation. Haze-I evolved from moderate (average $PM_{2.5}$: 76–108 $\mu g\,m^{-3}$) to heavy pollution (151–154 $\mu g\,m^{-3}$), with the dominant $PM_{2.5}$ component changing from organic matter (OM) (39–45 $\mu g\,m^{-3}$) to secondary inorganic ions (94–101 $\mu g\,m^{-3}$). Similarly, TEM observations showed that S-rich particles internally mixed with OM (named S-OM) increased from 29 % to 60 % by number at an urban site and 64 % to 74 % at a mountain site from the moderate Haze-I to heavy Haze-I events, and 75 %–96 % of Haze-I particles included primary OM. We found that change of wind direction caused Haze-I to rapidly turn into Haze-II (185–223 $\mu g\,m^{-3}$) with predominantly OM (98–133 $\mu g\,m^{-3}$) and unexpectedly high K^+ (3.8 $\mu g\,m^{-3}$). TEM also showed that K-rich particles internally mixed with OM (named K-OM) increased from 4 %–5 % by number to 50 %–52 %. The results indicate that there were different sources of aerosol particles causing the Haze-I and Haze-II formation: Haze-I was mainly induced by accumulation of primary OM emitted from residential coal burning and further deteriorated by secondary aerosol formation via heterogeneous reactions; Haze-II was caused by long-range transport of agricultural biomass burning emissions. Moreover, abundant primary OM particles emitted from coal and biomass burning were considered to be one typical brown carbon, i.e., tar balls. Our study highlights that large numbers of light-absorbing tar balls significantly contribute to winter haze formation in northeast China and they should be further considered in climate models.

1 Introduction

Haze pollution is mainly caused by high levels of fine particulate matter ($PM_{2.5}$), and it has spread widely over the globe to places such as Mexico City (Adachi and Buseck, 2008), Paris, France (Fortems – Cheiney et al., 2016), north India (Chowdhury et al., 2019), north China (Huang et al., 2014), and the Arctic (Frossard et al., 2011). In the past 20 years,

regional haze events with high concentrations of $PM_{2.5}$ have frequently occurred in China following rapid economic development. Various studies on regional haze in China have been conducted by many scientists (e.g., Bennartz et al., 2011; Guo et al., 2014; Li and Shao, 2009; Lin et al., 2017; M. Liu et al., 2017; Ren et al., 2016; Shi et al., 2017; Zhang et al., 2018b). Current hot issues on haze pollution concentrate on the formation processes of regional haze in various atmospheric environments and their potential optical and health influences (J. Chen et al., 2017; Gao et al., 2017).

Many of these studies reported that haze particles can adversely affect human health, ecological environments, and regional climate (Ding et al., 2016; Huang et al., 2013; Lelieveld et al., 2015; W. Li et al., 2017; Liu et al., 2019, 2016; Mahowald et al., 2018; Shi et al., 2019; Xie et al., 2019; Zhang et al., 2013). For example, exposure to high levels of ambient $PM_{2.5}$ cause or contribute to a variety of human diseases (e.g., stroke, ischemic heart disease, chronic obstructive pulmonary disease, and lung cancer) (Chen et al., 2019; Liu et al., 2016) and lead to $\sim$ 1.3 million premature deaths per year in China (Lelieveld et al., 2015). Abundant anthropogenic metal, ammonium, and phosphorus-containing particles are transported into remote regions of oceans, where they promote plankton growth and further influence ocean ecology (W. Li et al., 2017; Mahowald et al., 2018; Shi et al., 2019). High concentrations of fine aerosols suspended in haze layers not only influence regional climate through absorbing (e.g., black carbon (BC) and brown carbon (BrC)) and scattering (e.g., sulfates and nitrates) solar radiation (Huang et al., 2013; Liu et al., 2019; Xie et al., 2019), but also depress the planetary boundary layer development (Ding et al., 2016; Z. Li et al., 2017; Zhang et al., 2013) and reduce crop yields (Tie et al., 2016) in China. Therefore, understanding haze formation mechanisms and sources of haze particles in different regions of China is crucial to provide feasible control strategies for reducing regional $PM_{2.5}$ concentration and protecting ecosystems.

In China, regional heavy haze events frequently occur in the North China Plain (NCP) (Zhao et al., 2013) and northeast China (Ma et al., 2018) during winter. In the past decades, the regional haze formation mechanisms in the NCP have been intensely investigated (S. Chen et al., 2017; Cheng et al., 2016; Li et al., 2015; Y. Liu et al., 2017; Tao et al., 2014; Tian et al., 2015; G. Wang et al., 2016, 2019, 2014; Xing et al., 2019; G. J. Zheng et al., 2015; Zhong et al., 2019). Adverse meteorological conditions (e.g., low wind speeds and stable atmospheric boundary layer) can induce preliminary formation of haze during winter (G. J. Zheng et al., 2015; Zhong et al., 2019). Massive numbers of primary particles from industries, households, and vehicular exhaust emissions (e.g., fly ash, metal, primary organic matter, and soot particles) are the major aerosols in winter hazes (S. Chen et al., 2017; Tian et al., 2015; Wang et al., 2019). Rapid production of secondary aerosols (e.g., sulfates, nitrates, and secondary organics) via heterogeneous reactions under high relative humidity (RH) mainly elevates haze levels and causes regional hazes (X. Li et al., 2019; Y. Liu et al., 2017; G. Wang et al., 2016; Xing et al., 2019). The two-way feedback between accumulation of air pollutants and depression of the atmospheric boundary layer also aggravate haze pollution (Wang et al., 2014; Zhong et al., 2019). Moreover, regional transport of air pollutants is one of the important factors for the long duration of regional haze (Li et al., 2015; Tao et al., 2014; G. J. Zheng et al., 2015). These studies revealed formation mechanisms of regional winter hazes in the NCP well.

Among different regions or cities in China, the haze formation mechanisms would most likely differ due to different emissions and meteorological conditions (M. Li et al., 2019; Zhang et al., 2017; G. J. Zheng et al., 2015). The air quality in northeast China, a region with a long heating period (mid-October to mid-April), is mainly influenced by abundant inefficient combustion activities (e.g., coal and biomass burning in residential stoves and coal burning in small boilers for household heating and cooking) (Yang et al., 2017; Zhang et al., 2017). Extremely high concentrations of organic aerosols have been observed in northeast China during winter haze that coincides with crop growing and harvest periods (Cao et al., 2017; Chen et al., 2015; Zhang et al., 2017). Because of the influences of the regional haze in winter, annual aerosol optical depth in urban areas was $\sim$ 3.7 times higher than that in rural areas in northeast China (H. Zhao et al., 2018). In the past 5 years, some studies have focused on the physicochemical properties of haze particles collected in northeast China (Cao et al., 2017; Chen et al., 2015; X. Li et al., 2017; Miao et al., 2018; Zhang et al., 2017; H. Zhao et al., 2018). However, studies on regional haze evolution and haze formation mechanisms in northeast China are rare. This limited information precludes the comparison of regional hazes in northeast China with other regions in China. Furthermore, it is difficult to adopt some reasonable regional haze pollution control strategies from the NCP to apply to the air pollution in northeast China.

Northeast China is only one intense anthropogenic emission region in addition to Mongolia across the relatively high-latitude ($> 40^\circ$ N) areas on Earth (van Donkelaar et al., 2016). This region is significantly influenced by the Siberian cold, high-pressure systems in winter. The Siberian anticyclone transports air pollutants from northeast China to South Korea, Japan, and even the Arctic and further exerts large-scale influence in the global climate (Jung et al., 2015; Rodo et al., 2014; Sobhani et al., 2018; Zhang et al., 2016). Therefore, understanding the physicochemical characteristics of anthropogenic fine particles in regional haze and regional haze formation mechanisms over northeast China has to be considered of the utmost importance.

In this study, we conducted a field experiment in the south part of northeast China from 25 October to 6 November 2016. Two contrasting regional heavy-haze events occurred during 31 October–5 November 2016. We investi-

gated the types and mixing states of individual aerosol particles and $PM_{2.5}$ composition during these two events. Finally, we elucidated the formation mechanisms of two regional haze events and the main sources of fine haze particles.

2 Experimental methods

2.1 Sampling sites and sample collections

There are three provincial capital cities (i.e., Shenyang, Changchun, and Harbin) in northeast China that are surrounded by the Greater Khingan Mountains, the Lesser Khingan Mountains, and the Changbai Mountains (Fig. 1a). In this study, we selected an urban site (41.8° N, 123.35° E) and a mountain site (41.92° N, 123.65° E) in Shenyang (Fig. 1b). The urban site is located in the center of Shenyang. The mountain site on top of Qipan Mountain (224 m) is located ~ 30 km northeast of the urban site (Fig. 1b). There are only a few villages around Qipan Mountain, so its air quality represents the regional transport in the south part of northeast China well.

The $PM_{2.5}$ samples were collected on 90 mm quartz filters (Whatman, UK) using two medium-volume samplers (Wuhan Tianhong Instruments Co., TH-150A, 100 L min^{-1}) at the urban and mountain sites. Individual particle samples were collected on transmission electron microscopy (TEM) grids and silicon wafers using two DKL-2 samplers (Genstar Inc., 1 L min^{-1}) equipped with a 0.5 mm jet nozzle impactor at two sampling sites. The quartz filters provided mass concentrations and the chemical composition of ambient $PM_{2.5}$. The TEM grids and silicon wafers were used for microscopic observations of individual particles. To better explore the variation in $PM_{2.5}$ composition and individual particles, we collected the daytime (DT, 08:30–20:00 local time) $PM_{2.5}$ and nighttime (NT, 20:30–08:00 next day) $PM_{2.5}$ as well as individual particle samples four times a day (i.e., 00:00–03:00, 06:00–09:00, 12:00–15:00, and 18:00–21:00). To avoid individual particles overlapping on the substrate, the sampling duration of individual particles was varied from 30 s to 10 min depending on the $PM_{2.5}$ concentrations. In addition, we recorded the $PM_{2.5}$ concentrations reported by the nearby monitoring station during the sampling period and further compared them with our $PM_{2.5}$ data as shown in Table S1 in the Supplement. Although there is a 7 %–14 % deviation between these two datasets, the variations in $PM_{2.5}$ concentrations are the same (Table S1). Therefore, our $PM_{2.5}$ data can represent the condition of haze pollution during the sampling period. After individual particle samples were collected, we immediately used a portable optical microscope to check the particle distribution on the substrate, which guaranteed the sample to be suitable for microscopic analyses. After the sampling, the quartz filters were put into a −20 °C refrigerator and the TEM grids and silicon wafers were stored in the dry, clean, and airtight containers until laboratory analyses were performed.

Meteorological data (i.e., wind speed and wind direction, temperature, relative humidity (RH), and pressure) at the urban and mountain sites were simultaneously collected by two automated weather instruments (Kestrel 5500, USA) at 5 min intervals.

2.2 $PM_{2.5}$ analyses

The quartz filters are weighed with a high-precision digital balance (Sartorius ME 5-F, 0.001 mg of reading precision) after being equilibrated for 24 h under stable conditions (TP: 20 ± 1 °C; RH: 48 ± 2 %) before and after sampling. The $PM_{2.5}$ mass concentrations at the urban and mountain sites are calculated based on the weight difference and sampling volume of each quartz filter.

Each quartz filter collected at two sampling sites can be used to analyze chemical composition (i.e., water-soluble ions, organic carbon (OC), and elemental carbon (EC)) of $PM_{2.5}$. In this study, we use an ion chromatography system (Dionex ICS-90, USA) to obtain mass concentrations of water-soluble ions (i.e., Ca^{2+}, Mg^{2+}, K^+, Na^+, NH_4^+, NO_3^-, SO_4^{2-}, Cl^-, and F^-) and an OC–EC analyzer (Sunset Laboratory Inc., USA) to obtain mass concentrations of OC and EC. Concentrations of organic matter (OM) were further calculated through multiplying OC concentrations by a factor of 1.4 reported by Guinot et al. (2007). The experimental details about water-soluble ions analysis and OC–EC analysis have been provided in our previous study (Zhang et al., 2017).

2.3 TEM–EDS analysis

Individual particles on TEM grids (copper (Cu) grid covered by a carbon (C) reinforcement substrate) are examined using TEM combined with energy-dispersive X-ray spectrometry (EDS) (JEOL, JEM-2100). TEM observation provides the morphology of individual particles and the mixing states of different aerosol components in individual particles on the substrate. EDS determines the elemental composition of individual particles. EDS spectra of individual particles are collected within a maximum time of 30 s to minimize potential X-ray damage and ensure sufficient intensity during EDS analysis. Cu cannot be analyzed for individual particles because the TEM grids are made of Cu. In addition, the C content in EDS spectra of individual particles may be overestimated due to the substrate's contribution.

Individual particles are unevenly distributed on TEM grids, with coarser particles in the center of sampling spot and finer particles on the periphery. Therefore, to guarantee that the analyzed particles are representative, five areas are selected from the sampling center to periphery on each TEM grid. After a labor-intensive operation, a total of 3630 parti-

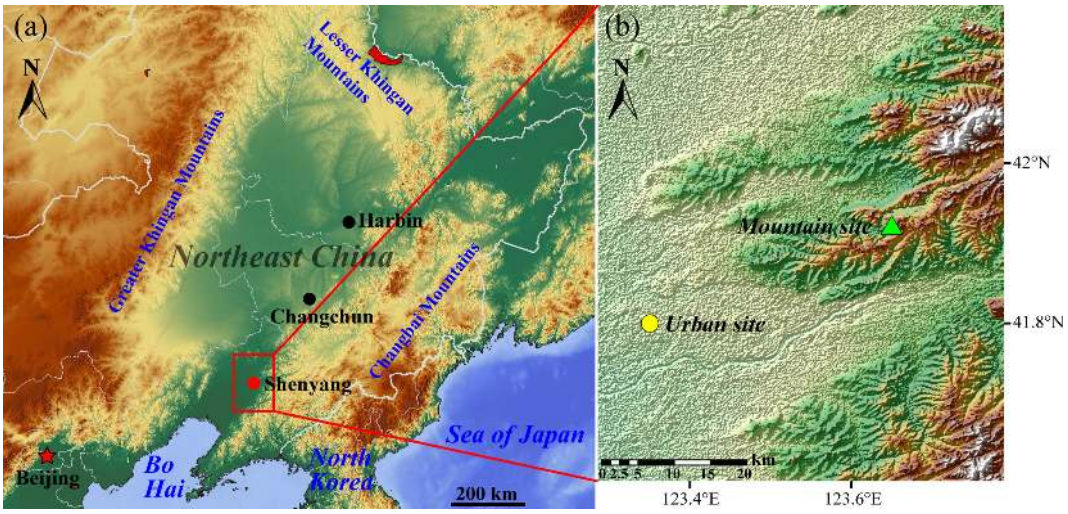

Figure 1. **(a)** Topographic features of northeast China, which is surrounded by the Greater Khingan Mountains, the Lesser Khingan Mountains, and the Changbai Mountains. **(b)** Locations of the urban and mountain sites. The relief map in **(a)** is from © OpenStreetMap contributors 2019 distributed under a Creative Commons BY-SA License (https://maps-for-free.com/, last access: 20 March 2020).

cles at the urban site and 4281 particles at the mountain site with a diameter $< 2.5\,\mu m$ were analyzed by TEM–EDS.

The area, perimeter, and equivalent circle diameter (ECD) of individual particles in TEM images are manually or automatically obtained through an image analysis software (iTEM, Olympus Soft Imaging Solutions GmbH, Germany).

2.4 NanoSIMS analysis

Based on TEM–EDS analysis, a representative individual particle sample is selected for the nanoscale secondary ion mass spectrometer (NanoSIMS, 50 L, CAMECA Instruments, Gennevilliers, France) analysis. In this work, signal intensity mapping of $^{12}C^{14}N^-$, $^{12}C^-$, $^{16}O^-$, and $^{32}S^-$ ions is obtained after the Cs^+ primary ion beam ionizes the atoms of the particle surface. Ion signal intensity mapping of individual particles with nanometer resolution clearly shows ion distribution in particles. Strong $^{12}C^{14}N^-$ and $^{12}C^-$ signals imply OM in individual particles and eliminate the contribution of C substrate on TEM grids (Chi et al., 2015).

2.5 AFM analysis

The surface structure of individual particles collected on silicon wafers is investigated using atomic force microscopy (AFM, Dimension Icon, USA) with a digital nanoscope IIIa in the tapping mode. AFM observations in the tapping mode produce 3-D images of individual particles. The tapping AFM is equipped with a cantilever and a conical tip with a 10 nm radius.

Based on the preliminary observations from TEM, we select three typical samples collected during the clean day, Haze-I event, and Haze-II event for the AFM analysis (the naming details for haze events are given in Sect. 3.1). To obtain the 3-D morphology of more particles on the basis of keeping images clear, a $10\,\mu m \times 10\,\mu m$ scanning range and 0.5–0.8 Hz scanning rate are selected. A total of 57 particles during the clean day and Haze-I and 29 particles during Haze-II were carefully analyzed. After obtaining AFM images of individual particles, we use the NanoScope Analysis software to automatically obtain the bearing area (A) and bearing volume (V) of each analyzed particle. The ECD and equivalent sphere diameter (ESD) of individual particles are further calculated according to the following two formulas.

$$A = \frac{4}{3}\pi r^2 = \frac{\pi d^2}{3} \rightarrow d = \sqrt{\frac{3A}{\pi}} \quad (1)$$

$$V = \frac{4}{3}\pi r^3 = \frac{4}{3} \times \frac{\pi D^3}{8} \rightarrow D = \sqrt[3]{\frac{6V}{\pi}} \quad (2)$$

Here d is ECD and D is ESD.

The linear correlations between ECD and ESD and typical AFM images of individual particles (clean day and Haze-I: $D = 0.5861 \times d$; Haze-II: $D = 0.4040 \times d$) are shown in Fig. S1a, b in the Supplement. Through the above two linear correlations, we can obtain the ESD of each individual particle analyzed by iTEM software.

3 Results

3.1 Composition of fine particles and meteorology

The concentrations of $PM_{2.5}$ and its chemical compositions during the sampling period are shown in Fig. S2. Regional haze pollution was observed in northeast China from 31 October to 5 November 2016 (Fig. S3). Based on the variation in $PM_{2.5}$ mass concentration and visibility at

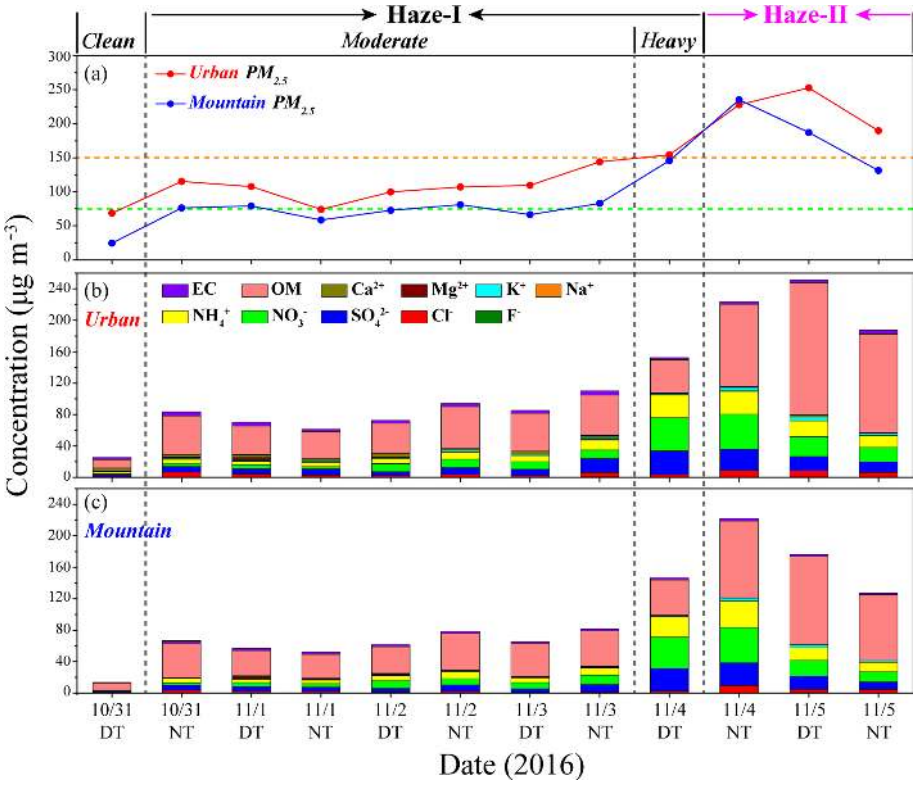

Figure 2. Variation in the concentrations of $PM_{2.5}$, organic matter (OM), elemental carbon (EC), and water-soluble ions (i.e., Ca^{2+}, Mg^{2+}, K^+, Na^+, NH_4^+, NO_3^-, SO_4^{2-}, Cl^-, and F^-) at the urban and mountain sites from daytime (DT) on 31 October to nighttime (NT) on 5 November 2016: **(a)** $PM_{2.5}$; **(b, c)** OM, EC, and water-soluble ions. Two regional haze episodes (Haze-I: 31 NT October–4 DT November; Haze-II: 4 NT–5 NT November) were identified.

the urban and mountain sites, clean days (31 DT October, $PM_{2.5} < 75\,\mu g\,m^{-3}$ and visibility > 10 km) and haze days (31 NT October–5 NT November, $PM_{2.5} \geq 75\,\mu g\,m^{-3}$ and visibility < 10 km) were identified (Fig. 2a). In general, we determined two regional haze events: 31 NT October–4 DT November (Haze-I) and 4 NT-5 NT November (Haze-II), based on the different prevailing wind directions (Haze-I: southerly; Haze-II: northerly) (Fig. S4a, b) and air mass backward trajectories (Fig. S5a).

To understand haze evolution, we divided the Haze-I event into a moderate haze stage (31 NT October–3 NT November) with $75\,\mu g\,m^{-3} \leq PM_{2.5} < 150\,\mu g\,m^{-3}$ and a heavy haze stage (4 DT November) with $PM_{2.5} \geq 150\,\mu g\,m^{-3}$ (Fig. 2a). Figure 2a shows that the average mass concentrations of $PM_{2.5}$ increased from 69 to $108\,\mu g\,m^{-3}$ at the urban site and from 25 to $76\,\mu g\,m^{-3}$ at the mountain site from the clean day to the moderate Haze-I event. Wind, RH, and pressure changed from northerly winds with 1.4 and $4.5\,m\,s^{-1}$, 35 % and 40 %, and 1034 and 1002 hPa at the urban and mountain sites on the clean day to southerly winds with 0.7 and $3.0\,m\,s^{-1}$, 39 % and 67 %, and 1022 and 991 hPa during the moderate Haze-I event, causing the occurrence of stable meteorological conditions (Fig. S4a–f). The average mass concentrations of OM, EC, and secondary inorganic ions (i.e., SO_4^{2-}, NO_3^-, and NH_4^+) in $PM_{2.5}$ increased from 11, 3.0, and $6\,\mu g\,m^{-3}$ during the clean day to 45, 4.3, and $24\,\mu g\,m^{-3}$ during the moderate Haze-I event at the urban site and from 9, 0.9, and $3\,\mu g\,m^{-3}$ to 39, 2.7, and $20\,\mu g\,m^{-3}$ at the mountain site, respectively (Fig. 2b, c). Following $PM_{2.5}$ concentration exceeding $150\,\mu g\,m^{-3}$, the moderate Haze-I event evolved into the heavy Haze-I event (Fig. 2a). During the heavy Haze-I event, mass concentrations of $PM_{2.5}$ were $154\,\mu g\,m^{-3}$ at the urban site and $151\,\mu g\,m^{-3}$ at the mountain site (Fig. 2a). RH remained high at 73 %–80 % at the urban and mountain sites during the heavy Haze-I event (Fig. S4c, d). Figure 2b, c show that the average concentrations of OM and EC were fairly constant at 39–45 and 2.7–4.3 $\mu g\,m^{-3}$ from the moderate Haze-I to the heavy Haze-I event. In contrast, secondary inorganic ions rapidly increased from 20–24 to 94–101 $\mu g\,m^{-3}$ in the DT of 4 November (Fig. 2b, c). Therefore, the variation in chemical composition of $PM_{2.5}$ clearly reflected the general haze evolution from moderate to heavy in northeast China.

With the prevailing wind changing from southerly with $\sim 0.8\,m\,s^{-1}$ to northerly with $\sim 3.9\,m\,s^{-1}$ (Fig. S4a, b), the Haze-I event turned into the Haze-II event. The average $PM_{2.5}$ concentrations remained at high levels and reached $223\,\mu g\,m^{-3}$ at the urban site and $185\,\mu g\,m^{-3}$ at the moun-

tain site (Fig. 2a). RH was consistently high in the range of 65 %–87 % during the Haze-II event (Fig. S4c, d). In addition, we noticed that hourly concentrations of $PM_{2.5}$ and CO rapidly climbed from 209 $\mu g\,m^{-3}$ and 1.3 ppm at 06:00 to 669 $\mu g\,m^{-3}$ and 1.9 ppm at 08:00 on 5 November, respectively (Fig. S6a, b). Although $PM_{2.5}$ concentrations during the Haze-II event were close to those of the heavy Haze-I event, we found large differences between aerosol chemistry in these two heavy-haze events besides the prevailing wind direction (Fig. 2a–c). From the heavy Haze-I to Haze-II events, secondary inorganic ions significantly decreased from 62 %–66 % of the total $PM_{2.5}$ mass (94–101 $\mu g\,m^{-3}$) to 31 %–35 % (65–70 $\mu g\,m^{-3}$), but OM markedly increased from 27 %–30 % (42–45 $\mu g\,m^{-3}$) to 53 %–60 % (98–133 $\mu g\,m^{-3}$) (Fig. 2a–c). In addition, K^+ average concentrations unexpectedly increased from 1.4 $\mu g\,m^{-3}$ during the heavy Haze-I event to 3.8 $\mu g\,m^{-3}$ during the Haze-II event (Fig. 2b, c). As a result, the difference between $PM_{2.5}$ composition before and after 4 November again proved that there were two different haze events under the different prevailing wind directions. These two regional haze events might have different formation mechanisms (details in Sect. 4.1).

3.2 Characteristics of individual haze particles

TEM–EDS did an excellent job of determining the morphology and composition of individual particles as shown in Fig. 3a–j. NanoSIMS was used to further identify OM particles through ion ($^{12}C^{14}N^-$, $^{12}C^-$, $^{16}O^-$, and $^{32}S^-$) signal mappings in order to exclude the interference of C substrate on TEM grids to EDS (Fig. 3k). Figure 3k shows high $^{12}C^{14}N^-$ and $^{12}C^-$ signals but low $^{32}S^-$ signal, which strongly confirms the OM particle. As a result, six basic types of aerosol components were classified based on their morphology, composition, and ion signal mapping: mineral, OM, soot (also known as EC and BC), fly ash/metal, S-rich particles, and K-rich particles (Fig. 3a–k).

Mineral particles mainly contain O, Si, Al, and Fe elements and present an irregular shape (Fig. 3a-1 and a-2). Mineral particles mainly occurred in the coarse size range (> 1 µm) (Fig. S7a, b), and they were often externally mixed with other types of particles (i.e., OM, soot, fly ash/metal, S-rich particles, and K-rich particles) (Fig. 3a-1). OM particles are mainly composed of C, O, and Si (Fig. 3b-2, c-2, and i-2). OM particles were further classified into spherical OM (Fig. 3b-1), domelike OM (Fig. 3c-1), and OM coating (Fig. 3i-1 and 3j) based on their morphology. TEM observations showed that most OM particles were internally mixed with S-rich (Fig. 3f-1), soot (Fig. 3g), and K-rich (Fig. 3i-1 and j) particles. Soot particles mainly include C and O elements and are aggregates of carbonaceous spheres (Fig. 3d-1 and d-2). Figure S7a, b show that soot particles mainly occurred in the fine size range (< 200 nm). TEM observations showed that a majority of soot particles were internally mixed with S-rich or OM particles, which were classified as soot–S/OM particles (Fig. 3g). Fly ash/metal particles with spherical morphology are mainly composed of O, Si, and metallic elements (e.g., Al, Fe, Mn, and Pb) (Fig. 3e-1 and e-2). Fly ash/metal particles were mainly in the ultrafine size range (< 100 nm) (Fig. S7a, b) and internally mixed with S-rich or OM particles, which were called fly ash/metal–S/OM particles (Fig. 3h). S-rich particles are mainly composed of O, S, and N (Fig. 3f-2) and formed from the oxidation of SO_2, NO_x, and NH_3. S-rich particles normally represent the mixtures of $(NH_4)_2SO_4$ and NH_4NO_3 (Li et al., 2016). TEM observations showed that abundant S-rich particles were internally mixed with OM particles, called S-OM particles (Fig. 3f-1). K-rich particles mainly contain K, O, S, and N elements (Fig. 3i-3). All K-rich particles were internally mixed with OM particles and were called K-OM particles (Fig. 3i-1 and j). To compare number fractions of OM particles during the haze evolution, here we considered the particles including OM as OM-containing particles. In the same way, soot-containing and fly ash/metal-containing particles were also defined.

Figure 4 shows the variation in number fractions of different particle types at the urban and mountain sites from the clean day to the Haze-I event and to the Haze-II event. At the urban site, these data show that mineral and S-OM were the major particle types, which accounted for 36 % and 23 % during the clean day. Subsequently, S-OM, OM, and soot-containing particles became major particle types which accounted for 29 %, 18 %, and 23 % at the urban site during the moderate Haze-I event. During the heavy Haze-I event, S-OM particles dominated at 60 % at the urban site (Fig. 4). Interestingly, we found that S-OM particles remained at very high frequencies (61 %–74 %) at the mountain site from the clean day to the Haze-I event (Fig. 4). Furthermore, the pink frames in Fig. 4 show that OM-containing (i.e., S-OM, OM, soot-OM, fly ash/metal-OM, and K-OM) particles accounted for 75 %–86 % at the urban site and 95 %–96 % at the mountain site during the Haze-I event. During the Haze-II event, number fractions of OM-containing particles reached their maximum at 96 % at the urban site and 97 % at the mountain site (Fig. 4). It is noted that K-OM became the predominant particles in the Haze-II event, accounting for 50 % at the urban site and 52 % at the mountain site (Fig. 4). Therefore, individual particle analysis clearly shows large differences of particle types and fractions following the haze evolution, which is consistent with the variation in $PM_{2.5}$ composition described in Sect. 3.1.

3.3 Pollutants change following haze evolution and transformation

The analysis of X/EC (e.g., $PM_{2.5}$/EC, OC/EC, SO_4^{2-}/EC, NO_3^-/EC, and K^+/EC) factors not only can exclude the influence of changes in atmospheric boundary layer height on pollutant mass concentrations, but also can indicate accumu-

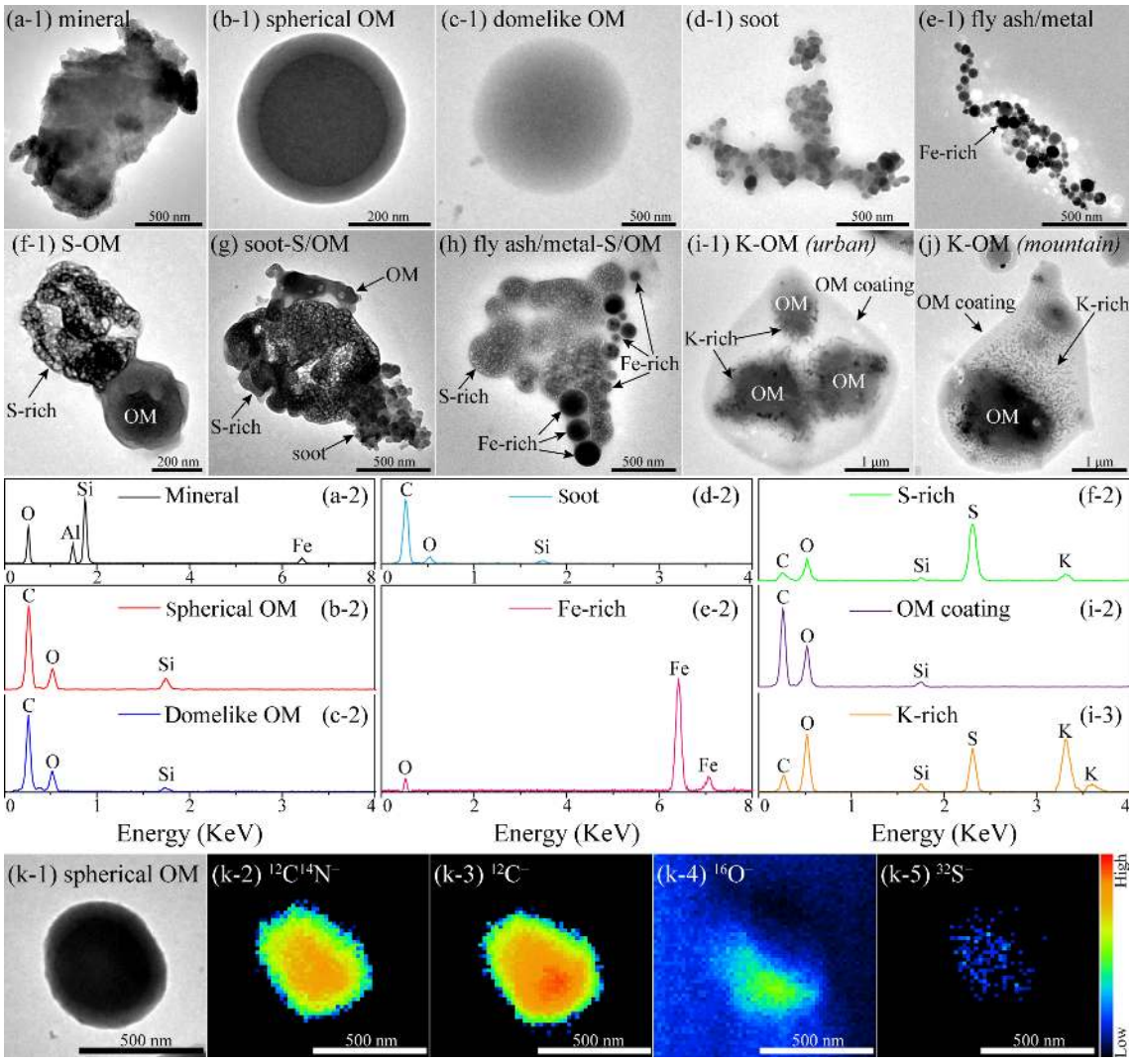

Figure 3. Typical transmission electron microscopy (TEM) images and energy-dispersive X-ray spectrometry (EDS) spectra of different types of individual aerosol particles: **(a)** mineral particle; **(b)** spherical OM particle; **(c)** domelike OM particle; **(d)** soot particle; **(e)** Fe-rich particle; **(f)** mixture of S-rich and OM particles; **(g)** mixture of soot, S-rich, and OM particles; **(h)** mixture of Fe-rich and S-rich particles; **(i, j)** mixture of K-rich and OM particles at the urban and mountain sites. The EDS spectra of these particle components are located below their TEM images. **(k)** A typically spherical OM particle and its NanoSIMS ion intensity mappings of $^{12}C^{14}N^-$, $^{12}C^-$, $^{16}O^-$, and $^{32}S^-$ signals. Particles in **(a–h, k)** and **(i, j)** were collected during the Haze-I and Haze-II events, respectively.

lation (e.g., small changes in X/EC) and secondary formation (e.g., increases in SO_4^{2-}/EC and NO_3^-/EC) of $PM_{2.5}$ during haze evolution (Zhang et al., 2017; G. J. Zheng et al., 2015). Although $PM_{2.5}$ concentrations increased from 69 to 108 $\mu g\,m^{-3}$ at the urban site and from 25 to 76 $\mu g\,m^{-3}$ at the mountain site from the clean day to the moderate Haze-I event, X/EC factors only displayed minor variations (Fig. 5a, b). This result shows that accumulation of air pollutants under stable meteorological conditions (Fig. S4a–f) mainly induced the moderate Haze-I formation. Following formation of the heavy Haze-I event with $PM_{2.5}$ concentrations at 154 $\mu g\,m^{-3}$ at the urban site and 151 $\mu g\,m^{-3}$ at the mountain site, SO_4^{2-}/EC, NO_3^-/EC, and $PM_{2.5}$/EC factors dramatically increased (Fig. 5a, b). Figure 5a, b show that SO_4^{2-}/EC and NO_3^-/EC factors reached their maximum values at the two sampling sites during the heavy Haze-I event, suggesting that secondary sulfates and nitrates significantly increased during Haze-I evolution (details in Sect. 4.1). In contrast, SO_4^{2-}/EC and NO_3^-/EC factors began to decrease, but OC/EC, K^+/EC, and $PM_{2.5}$/EC factors significantly increased during the Haze-II event, although $PM_{2.5}$ concentrations became even further elevated to 223 $\mu g\,m^{-3}$ at the urban site and 185 $\mu g\,m^{-3}$ at the mountain site (Fig. 5a, b). This result indicates that large amounts of aerosol including OM and K^+ contributed to the conversion from the Haze-I to the Haze-II events (details in Sect. 4.1).

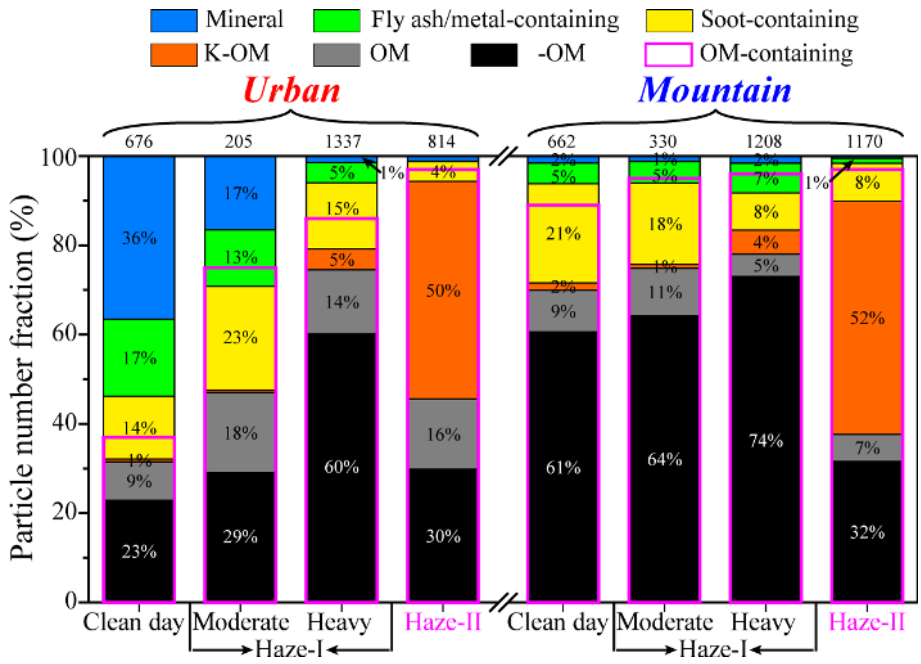

Figure 4. Variation in number fractions of different types of particles at the urban and mountain sites. Analyzed particle numbers are listed at the top of each bar.

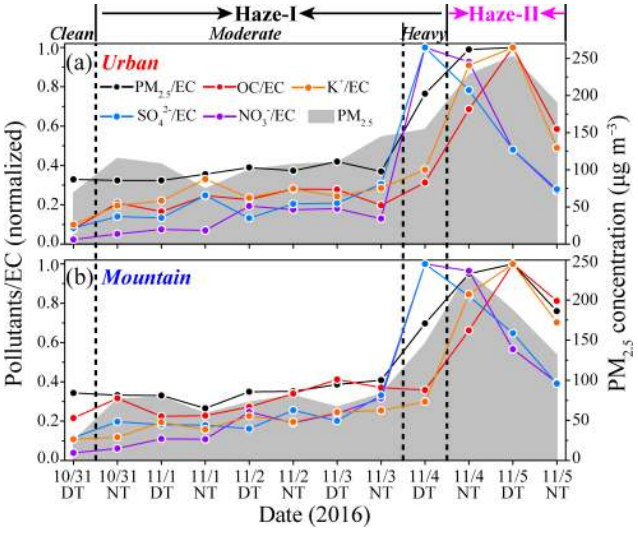

Figure 5. Variation in $PM_{2.5}$/EC, OC/EC, SO_4^{2-}/EC, NO_3^-/EC, and K^+/EC factors at the urban site **(a)** and mountain site **(b)**. These factors are normalized.

Individual particle analysis shows consistent results with the variation in X/EC factors described above: the fractions of OM, S-OM, and soot-containing particles only had minor changes of 6 %–9 % (i.e., 9 % to 18 %, 23 % to 29 %, and 14 % to 23 %) at the urban site and 2 %–3 % (i.e., 9 % to 11 %, 61 % to 64 %, and 21 % to 18 %) at the mountain site from the clean day to the moderate Haze-I event (Fig. 4). However, along with the moderate Haze-I evolving into the heavy Haze-I event, S-OM fractions suddenly increased from 29 % to 60 % at the urban site and from 64 % to 74 % at the mountain site (Fig. 4). When the heavy Haze-I turned into the Haze-II events, S-OM fractions significantly decreased from 60 %–74 % to 30 %–32 % at two sampling sites, but K-OM fractions largely increased from 4 %–5 % to 50 %–52 % (Fig. 4). As a result, the chemical data of $PM_{2.5}$ samples and individual particle analysis both reflect the haze evolution and transformation well.

4 Discussion

4.1 Sources and formation of two distinctive haze events

Our analyses show that the fractions of OM in $PM_{2.5}$ by mass (35 %–41 %, Fig. 2a–c) and OM contained in individual particles by number (> 70 %, Fig. 4) were both elevated during the Haze-I event at the urban and mountain sites. TEM observations showed two major types of OM particles during the Haze-I event: spherical OM and domelike OM (Fig. 6c, d), which were not frequently observed during summer haze events influenced by industries, coal-fired power plants, and vehicle exhaust (Li et al., 2016; Yuan et al., 2015). Therefore, large numbers of spherical OM and domelike OM particles did not come from the emissions of industry, coal-fired power plants, and vehicle exhaust. Moreover, the similar OM particles have been considered primary OM aerosols and they can be directly emitted from residential coal burning (Zhang

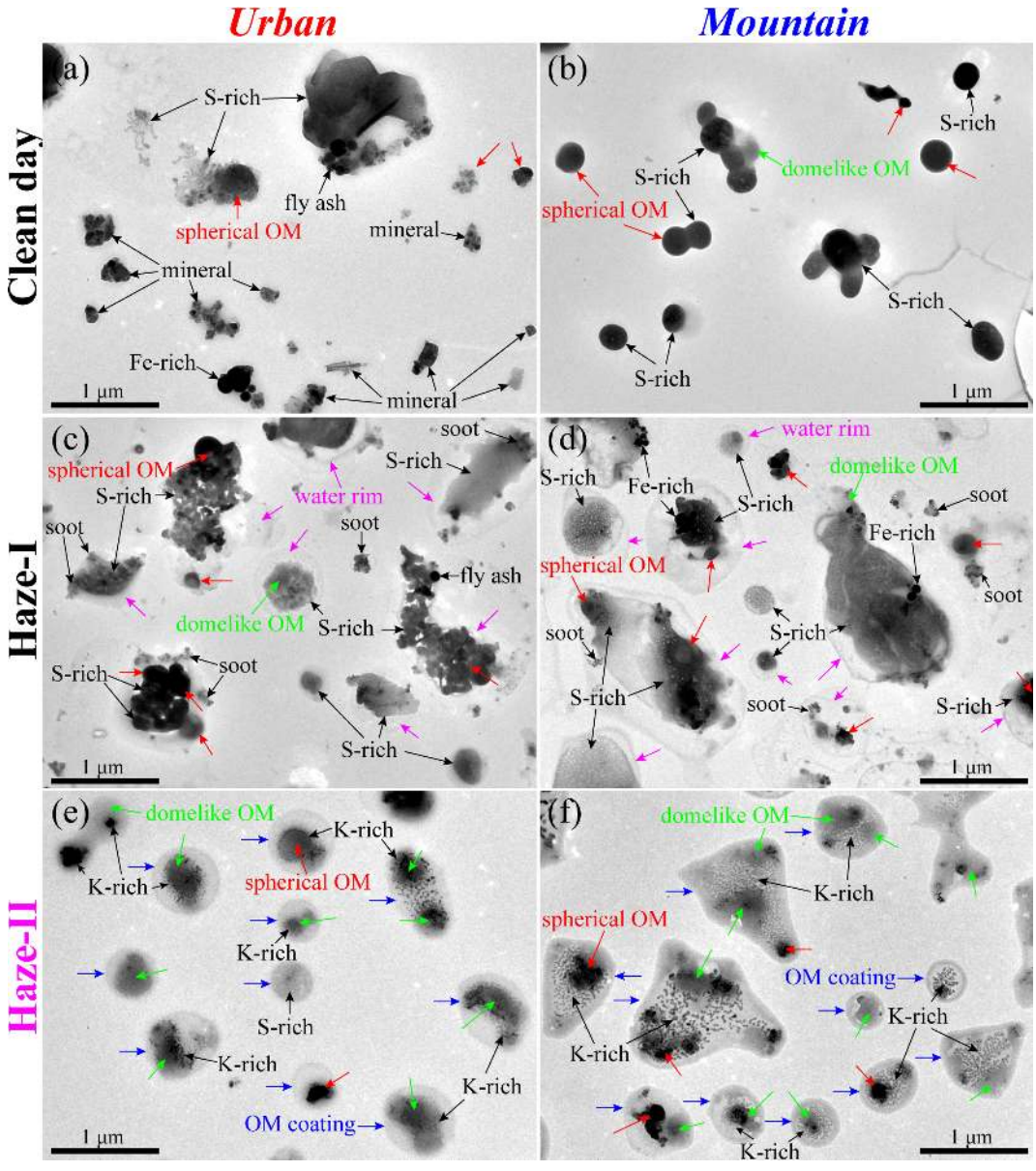

Figure 6. Typical TEM images of individual aerosol particles at low magnification at the urban and mountain sites: **(a, b)** clean day; **(c, d)** Haze-I; **(e, f)** Haze-II. The red, green, blue, and pink arrows represent spherical OM, domelike OM, OM coating, and water rim, respectively.

et al., 2018a) or biomass burning (L. Liu et al., 2017). Many studies found that many haze events caused by biomass burning contained high levels of K^+ at 2.8–5.8 $\mu g\,m^{-3}$ (Cao et al., 2016; Cheng et al., 2013; Huang et al., 2012; H. Li et al., 2010) and K-OM particles at 10 %–60 % by number (W. J. Li et al., 2010; Pósfai et al., 2003; H. Wang et al., 2016). However, our results showed quite low K^+ concentration at 1.1 $\mu g\,m^{-3}$ (Fig. 2b, c) and only 3 % K-OM (Fig. 4) as well as poor correlations with K-OM fractions and $PM_{2.5}$ concentrations (Fig. 7a) during the Haze-I event. The results suggest that biomass burning was not one major source during the Haze-I event. Therefore, we can exclude biomass burning and conclude that coal burning was the major emission source during the Haze-I event. During the wintertime with the lowest temperature of about −30 °C in northeast China, high-intensity coal burning for household heating is necessary (Yang et al., 2017; Zhang et al., 2017). Central heating via large boilers equipped with efficient filters is in wide use in the urban areas in northeast China, but large numbers of residential stoves without emission controls are still used for household heating and cooking using burning coals in the rural and suburban areas that do emit abundant primary OM

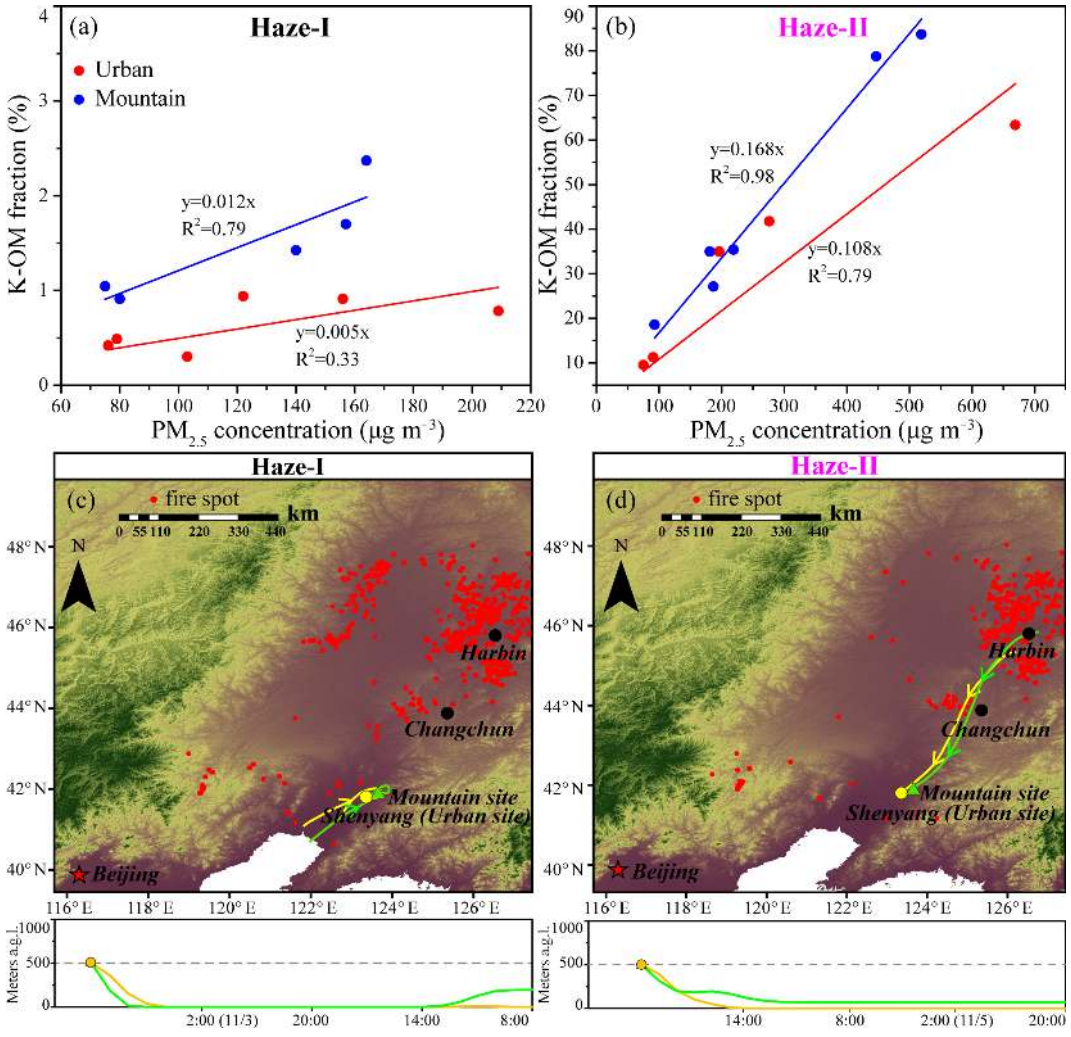

Figure 7. Linear correlations between $PM_{2.5}$ mass concentration (x) and K-OM number fraction (y) during Haze-I **(a)** and Haze-II **(b)**. Typical 24 h air mass backward trajectories before arriving at the urban and mountain sites during Haze-I **(c)** and Haze-II **(d)**. Fire spot data are from the MODIS Collection 6 active fire product provided by NASA FIRMS (https://firms.modaps.eosdis.nasa.gov/map/, last access: 20 March 2020).

particles (Xu et al., 2017; Zhang et al., 2017). Through the meteorological data (Fig. S4a, b), air mass backward trajectory (Fig. 7c), and concentration-weighted trajectory (CWT) plots of $PM_{2.5}$ (Fig. S5b–d) analyses, we inferred that the air quality at the two sampling sites during the Haze-I event was mostly influenced by Shenyang and its nearby surrounding emissions, although transport from the Beijing–Tianjin–Hebei region slightly contributed to the heavy Haze-I formation on 4 DT November. In a word, we determined that large amounts of fine primary OM aerosol during the Haze-I event were mainly from regional emissions of coal burning in residential stoves for heating and cooking as shown in Fig. 8.

The significant increases in SO_4^{2-}/EC, NO_3^-/EC, and $PM_{2.5}$/EC factors from the moderate to heavy Haze-I event (Fig. 5a, b) suggest that massive secondary production of sulfates and nitrates elevated $PM_{2.5}$ concentrations. Figure S5c, d further indicate that compared with transport from the Beijing–Tianjin–Hebei region local secondary transformation was one major factor to cause the heavy Haze-I formation. Similar results that secondary aerosol formation causes heavy winter hazes in the NCP have been well documented (Y. Liu et al., 2017; Sun et al., 2014; Xue et al., 2016; B. Zheng et al., 2015). Because of low O_3 levels at 12 ppb (Fig. S6d) and a fair thick haze layer weakening solar radiation (Zhao et al., 2013; G. J. Zheng et al., 2015) during the heavy Haze-I event, photochemical activity should be ignored in the air, and heterogeneous chemical reactions on particle surfaces can be considered major pathways in the formation of sulfates and nitrates from SO_2 and NO_x whenever RH exceeds 70 % (Sun et al., 2018; G. Wang et al., 2016; Wu et al., 2018). Here, TEM observations did show that the heavy Haze-I particles were wet aerosols and presented a

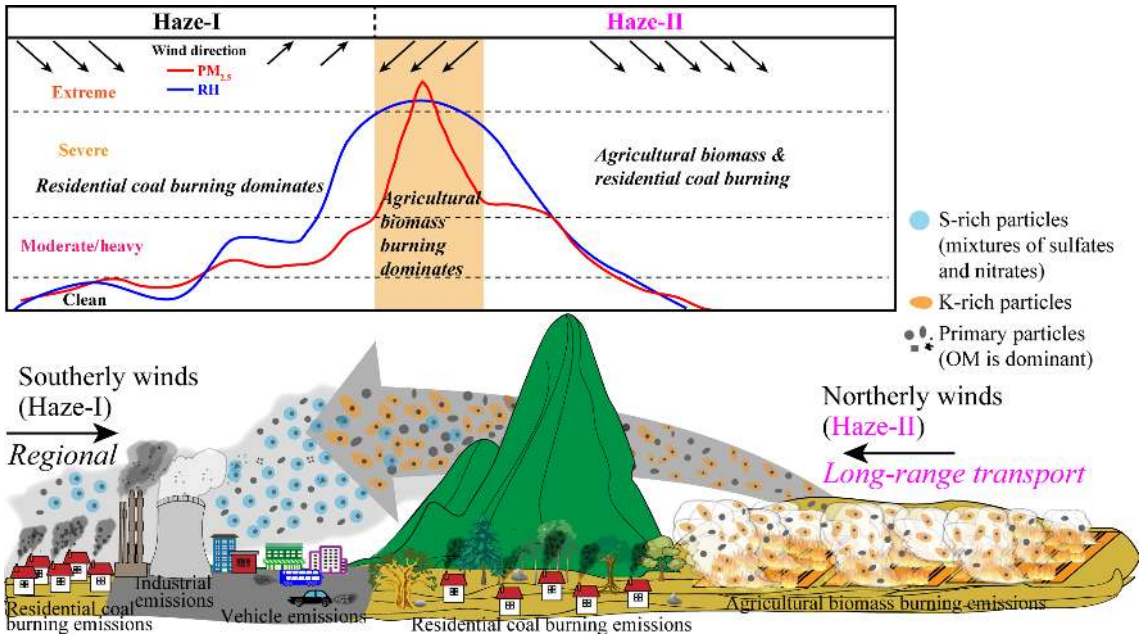

Figure 8. Schematic diagram of Haze-I and Haze-II formation in northeast China during winter. The major emission sources and haze formation processes are shown.

S-rich coating on primary OM, soot, or fly ash/metal particles at 73 %–80 % RH (Figs. 6c, d and S4c, d). Obviously, the preexisting particles in the haze provided large heterogeneous surfaces for the formation of sulfates and nitrates (He et al., 2014; Li et al., 2011; G. Wang et al., 2016). When the moderate Haze-I turned into the heavy Haze-I event, we indeed found that secondary inorganic ions (i.e., SO_4^{2-}, NO_3^-, and NH_4^+) became the predominant species in $PM_{2.5}$, accounting for 62 %–66 % (Fig. 2a–c). Therefore, we concluded that atmospheric heterogeneous reactions under high RH (> 70 %) and local primary emissions together induced the heavy Haze-I formation in northeast China.

In contrast to the Haze-I event, we found that concentrations of K^+ and OM in $PM_{2.5}$ were both about twice as much during the Haze-II event (Fig. 2b, c). In addition, TEM observations showed that the fraction of K-OM particles explosively increased by 45 %–48 % during the Haze-II event (Fig. 4). High levels of K^+ or K-OM particles represent the influences of biomass burning (Bi et al., 2011; L. Liu et al., 2017). Indeed, MODIS data during the Haze-II event show that many fire spots occurred in the north part of northeast China, ∼ 580 km from sampling sites, and the air mass backward trajectories at the urban and mountain sites both crossed these fire spots (Fig. 7d). MODIS maps further show that these fire spots were in farmland instead of the forest areas (Fig. 7d). Based on the MODIS data and reports from the local department of ecology and environment (http://www.hljdep.gov.cn/hjgl/zfjc/jphz/2017/05/15698.html, last access: 20 March 2020), these dense fire spots on 4 November were agricultural biomass burning. Open agricultural biomass burning is normally intense during the early winter in northeast China, a region with abundant agricultural production, because large amounts of agricultural waste need to be cleaned up and their burned products can be used as fertilizer to increase soil fertility (Cao et al., 2017; Yang et al., 2017). Along with the backward trajectories of air masses, we found sharp $PM_{2.5}$ concentrations occurring from Harbin (1281 µg m^{-3} at 18:00 on 4 November) to Changchun (658 µg m^{-3} at 00:00 on 5 November) and to Shenyang (669 µg m^{-3} at 08:00 on 5 November) (Fig. S6a). These above analyses indicated that long-range transport of agricultural biomass burning emissions directly led to the Haze-II formation (Fig. 8) and explained why K^+/EC, OC/EC, and $PM_{2.5}$/EC factors together reached their maximum values during the Haze-II event (Fig. 5a, b), and K-OM fractions and $PM_{2.5}$ mass concentrations had strong positive correlation (Fig. 7b). Overall, although the Haze-II and Haze-I events both displayed heavy pollution levels, they had contrasting emission sources and formation mechanisms as illustrated in Fig. 8. The above formation mechanisms of two haze events are similar to previous studies through radar observation (Zhong et al., 2019) and model simulation (Yang et al., 2017). These studies indicated that adverse meteorological conditions (e.g., low wind speed and high RH) and high-intensity emissions of residential heating and biomass burning mainly contributed to the haze formation in northeast China in winter. In addition, our previous study suggested that heterogeneous reactions were one major factor for regional winter haze evolution in northeast China (Zhang et al., 2017). Therefore, we confirmed these two continuous

haze events as typical haze pollution occurring in northeast China during winter.

4.2 Comparison: haze in northeast China vs. the North China Plain

Average OC/EC ratios in $PM_{2.5}$ of 8.0–10.6 during the Haze-I event and 25.4–27.9 during the Haze-II event were reported in northeast China in this study (Table S2). The results are much higher than OC/EC ratios in $PM_{2.5}$ during winter haze events in the NCP, such as 4.5 in Beijing (Zhao et al., 2013), 5.5 in Jinan (S. Chen et al., 2017), and 5.3 in Tianjin (Han et al., 2014). In addition, TEM observations showed that OM-containing particles were dominant by number fraction (e.g., 75 %–96 % during the Haze-I event and 96 %–97 % during the Haze-II event) in northeast China (Fig. 4). The results are higher than 50 %–70 % during regional haze events in the NCP which were influenced by residential coal burning (S. Chen et al., 2017; Li et al., 2012). These comparisons suggest that the contribution of residential coal burning and biomass burning to winter haze formation in northeast China is significantly larger than that in the NCP. Moreover, fly ash/metal-containing particles as the tracers of industry emissions frequently occurred in regional haze in the NCP, such as $\sim$ 30 % by number fraction in Jinan (Li et al., 2011), 23 %–29 % in Beijing (Ma et al., 2016), and 13 %–17 % in Xianghe (Zou et al., 2019). These data are much higher than 8 % (Haze-I) and 1 % (Haze-II) reported in this study (Fig. 4), suggesting that the contribution of industrial emissions to regional haze in northeast China is much smaller than that in the NCP. Many studies have summarized formation mechanisms of general regional haze in north China: regional transport of air pollutants (G. J. Zheng et al., 2015), massive formation of secondary aerosols (Shao et al., 2019), and two-way feedback between adverse meteorological conditions and pollutant accumulation (Zhong et al., 2019). We found that the Haze-I formation in this study can be attributed to these three formation mechanisms (Fig. 8). Moreover, the Haze-II formation indicates that the primary emissions from intensive agricultural biomass burning activities can rapidly induce regional heavy haze formation in northeast China (Fig. 8).

5 Atmospheric and health implications

High concentrations of $PM_{2.5}$ in haze adversely affect human health by inducing various respiratory diseases (Cohen et al., 2017; Liu et al., 2016). In China, long-term exposure to high levels of ambient $PM_{2.5}$ has resulted in 1.1–1.35 million premature deaths (Cohen et al., 2017; Lelieveld et al., 2015). Large-scale coal burning for household heating and cooking in northeast China emits vast numbers of OM-containing particles (discussed in Sect. 4.1), which include abundant polycyclic aromatic hydrocarbons (PAHs) (S. Chen et al., 2017; Chen et al., 2013; Zhang et al., 2008). Based on Ebenstein et al. (2017), people's life expectancy decreases by 0.64 years for every 10 $\mu g\,m^{-3}$ of PM_{10} contributed by residential coal burning emissions. Furthermore, we found that 1 %–8 % of haze particles contained toxic metals (e.g., Pb, Zn, Cr, and Mn) from fly ash/metal particles with sizes smaller than 100 nm in northeast China (Figs. 4 and S7a, b). Oberdorster et al. (2004) indicated that such ultrafine metal particles can have adverse health impacts via deposition in human lungs and further penetration into the blood. Therefore, these OM-containing and fly ash/metal-containing particles observed by TEM (Fig. 6a–f) are harmful to human health in northeast China in winter.

The light-absorbing particles (i.e., BC and BrC) have been proven to reduce solar radiation reaching the ground and further influence regional climate and crop production (Alexander et al., 2008; Bond et al., 2013; Tie et al., 2016; Wang et al., 2018). This study shows that concentrations of BC (i.e., EC or soot) were low at 2.7–4.3 $\mu g\,m^{-3}$ during the haze days and only accounted for 1.4 %–3.9 % of $PM_{2.5}$ in northeast China (Fig. 2a–c). These results are lower than those in other regions of China such as the NCP (7.6 $\mu g\,m^{-3}$ and 5.2 % in Beijing; Wu et al., 2016), Yangtze River Delta (11.8 $\mu g\,m^{-3}$ and 4.4 % in Shanghai; Zhi et al., 2014), and Pearl River Delta (9.6 $\mu g\,m^{-3}$ and 7.7 % in Guangzhou; Tao et al., 2012). These comparisons indicate that BC concentrations are at low levels in northeast China during winter haze periods, although $PM_{2.5}$ concentrations are extremely high. Furthermore, TEM observations showed that 75 %–97 % of haze particles were OM-containing particles such as spherical OM and domelike OM, but only 4 %–23 % were soot-containing particles in northeast China (Fig. 4). Previous studies have demonstrated that these spherical and domelike OM particles from coal and biomass burning with low combustion efficiency are tar balls (Chakrabarty et al., 2010; Hand et al., 2005; Pósfai et al., 2004; Zhang et al., 2018a) or precursors of tar balls (Adachi et al., 2019; Sedlacek et al., 2018; Tóth et al., 2014), respectively. Tar balls as the primary BrC have a wide absorption spectrum from visible to ultraviolet wavelengths (Hoffer et al., 2016). The comparison in Sect. 4.2 indicates that the highest emission of tar balls in China during winter occurs in northeast China because of the intense and inefficient residential coal burning and agricultural biomass burning. Therefore, how large numbers of tar balls in regional winter haze influence atmospheric optical radiation and climate in northeast China should be studied in much greater detail.

Implementing suitable policies to encourage cleaner energy use (e.g., natural gas and electricity) instead of coal and biomass for household heating is necessary in northeast China. Such policies would not only reduce regional haze formation but also reduce the toxic aerosol components in the air. Admittedly, this transition of heating energy would face a monumental challenge in northeast China due to its low economic growth and its low urbanization development

rates (B. Zhao et al., 2018). Moreover, how to control open agricultural biomass burning should be considered in northeast China. Over the past decades, agricultural biomass returned to soils and recycling agricultural biomass have both failed in northeast China. This failure arises because agricultural biomass does not decay throughout the winter with low temperatures down to −30 °C and snow or ice cover, and recycling biomass consumes a lot of manpower, material resources, and money (Yan et al., 2006). Therefore, how to deal with agricultural biomass waste in northeast China should be carefully thought out by the local farmers in concert with the government.

6 Conclusions

To understand the formation mechanisms of winter haze in northeast China, we carried out an aerosol experiment at an urban site and a mountain site in the south part of northeast China from 25 October to 6 November 2016. Two different regional heavy haze events (Haze-I and Haze-II) were identified during 31 October–5 November. Chemical composition (water-soluble ions, OM, and EC) of $PM_{2.5}$ was obtained using ion chromatography and OC/EC analysis. Types and mixing states of individual particles were identified using TEM / EDS and NanoSIMS: mineral, fly ash/metal-containing, soot-containing, OM, S-OM, K-OM, and OM-containing.

The Haze-I event has an evolution process from moderate to heavy pollution. OM was the dominant component in $PM_{2.5}$ and its concentrations were $45\,\mu g\,m^{-3}$ at the urban site and $39\,\mu g\,m^{-3}$ at the mountain site during the moderate Haze-I event. Individual particle analysis also showed that over 70 % of particles contained OM during the moderate Haze-I event. Following the Haze-I evolution, secondary inorganic ions (i.e., SO_4^{2-}, NO_3^-, and NH_4^+) became the dominant components (94–101 $\mu g\,m^{-3}$) during the heavy Haze-I event with $PM_{2.5}$ concentrations of 151–154 $\mu g\,m^{-3}$. Similarly, the number fractions of S-OM increased from 29 % to 60 % at the urban site and from 64 % to 74 % at the mountain site from the moderate Haze-I to the heavy Haze-I event. Along with the prevailing wind suddenly changing from southerly with $\sim 0.8\,m\,s^{-1}$ to northerly with $\sim 3.9\,m\,s^{-1}$, the heavy Haze-I event rapidly turned into the Haze-II event with $PM_{2.5}$ concentrations of 185–223 $\mu g\,m^{-3}$. Meanwhile, OM replaced secondary inorganic ions as the dominant component in $PM_{2.5}$ during the Haze-II event, accounting for 53 %–60 %. Furthermore, K^+ concentration during the Haze-II event was about 3 times higher than that during the heavy Haze-I event. Individual particle analysis showed consistent results, with the number fractions of K-OM significantly increasing from 4 %–5 % to 50 %–52 %.

Based on our study, the accumulation of primary OM particles, mainly emitted from residential coal burning, induced the moderate Haze-I formation with the onset of stable meteorological conditions. Production of secondary aerosols via heterogeneous reactions at high RH (> 70 %) and local primary emissions caused the transition from the moderate Haze-I to the heavy Haze-I events. Furthermore, the long-range transport of primary emissions from intense agricultural biomass burning led to the Haze-II formation in the downwind areas in northeast China. Our study also reveals that the significant light-absorbing particles in northeast China during winter are tar balls, which is different from other regions in China influenced by serious air pollution.

Data availability. All data presented in this paper are available upon request from the corresponding author (liweijun@zju.edu.cn).

Supplement. The supplement related to this article is available online at: https://doi.org/10.5194/acp-20-5355-2020-supplement.

Author contributions. JZ and WL conceived the study and wrote the manuscript. The field campaign was organized and supervised by WL, and LL, LX, and HZ assisted. JZ, LL, LX, and QL contributed the sample analyses. All authors reviewed and commented on the paper.

Competing interests. The authors declare that they have no conflict of interest.

Special issue statement. This article is part of the special issue "Multiphase chemistry of secondary aerosol formation under severe haze". It is not associated with a conference.

Acknowledgements. We appreciate Peter Hyde's comments on and proofreading of a previous version of the paper. We thank Jiaxing Sun and Yong Ren for their assistance in sample collections.

Financial support. This research has been supported by the National Key R&D Program of China (grant no. 2017YFC0212700), the National Natural Science Foundation of China (grant nos. 91844301, 41622504, and 41575116), the Zhejiang Provincial Natural Science Foundation of China (grant no. LZ19D050001).

Review statement. This paper was edited by Jingkun Jiang and reviewed by two anonymous referees.

References

Adachi, K. and Buseck, P. R.: Internally mixed soot, sulfates, and organic matter in aerosol particles from Mexico City, Atmos. Chem. Phys., 8, 6469–6481, https://doi.org/10.5194/acp-8-6469-2008, 2008.

Adachi, K., Sedlacek, A. J., Kleinman, L., Springston, S. R., Wang, J., Chand, D., Hubbe, J. M., Shilling, J. E., Onasch, T. B., Kinase, T., Sakata, K., Takahashi, Y., and Buseck, P. R.: Spherical tarball particles form through rapid chemical and physical changes of organic matter in biomass-burning smoke, P. Natl. Acad. Sci. USA, 116, 19336–19341, https://doi.org/10.1073/pnas.1900129116, 2019.

Alexander, D. T. L., Crozier, P. A., and Anderson, J. R.: Brown carbon spheres in East Asian outflow and their optical properties, Science, 321, 833–836, https://doi.org/10.1126/science.1155296, 2008.

Bennartz, R., Fan, J., Rausch, J., Leung, L. R., and Heidinger, A. K.: Pollution from China increases cloud droplet number, suppresses rain over the East China Sea, Geophys. Res. Lett., 38, L09704, https://doi.org/10.1029/2011GL047235, 2011.

Bi, X., Zhang, G., Li, L., Wang, X., Li, M., Sheng, G., Fu, J., and Zhou, Z.: Mixing state of biomass burning particles by single particle aerosol mass spectrometer in the urban area of PRD, China, Atmos. Environ., 45, 3447–3453, https://doi.org/10.1016/j.atmosenv.2011.03.034, 2011.

Bond, T. C., Doherty, S. J., Fahey, D. W., Forster, P. M., Berntsen, T., DeAngelo, B. J., Flanner, M. G., Ghan, S., Kärcher, B., Koch, D., Kinne, S., Kondo, Y., Quinn, P. K., Sarofim, M. C., Schultz, M. G., Schulz, M., Venkataraman, C., Zhang, H., Zhang, S., Bellouin, N., Guttikunda, S. K., Hopke, P. K., Jacobson, M. Z., Kaiser, J. W., Klimont, Z., Lohmann, U., Schwarz, J. P., Shindell, D., Storelvmo, T., Warren, S. G., and Zender, C. S.: Bounding the role of black carbon in the climate system: A scientific assessment, J. Geophys. Res.-Atmos., 118, 5380–5552, https://doi.org/10.1002/jgrd.50171, 2013.

Cao, F., Zhang, S. C., Kawamura, K., and Zhang, Y. L.: Inorganic markers, carbonaceous components and stable carbon isotope from biomass burning aerosols in Northeast China, Sci. Total Environ., 572, 1244–1251, https://doi.org/10.1016/j.scitotenv.2015.09.099, 2016.

Cao, F., Zhang, S. C., Kawamura, K., Liu, X., Yang, C., Xu, Z., Fan, M., Zhang, W., Bao, M., Chang, Y., Song, W., Liu, S., Lee, X., Li, J., Zhang, G., and Zhang, Y. L.: Chemical characteristics of dicarboxylic acids and related organic compounds in $PM_{2.5}$ during biomass-burning and non-biomass-burning seasons at a rural site of Northeast China, Environ. Pollut., 231, 654–662, https://doi.org/10.1016/j.envpol.2017.08.045, 2017.

Chakrabarty, R. K., Moosmüller, H., Chen, L.-W. A., Lewis, K., Arnott, W. P., Mazzoleni, C., Dubey, M. K., Wold, C. E., Hao, W. M., and Kreidenweis, S. M.: Brown carbon in tar balls from smoldering biomass combustion, Atmos. Chem. Phys., 10, 6363–6370, https://doi.org/10.5194/acp-10-6363-2010, 2010.

Chen, C., Li, H., Niu, Y., Liu, C., Lin, Z., Cai, J., Li, W., Ge, W., Chen, R., and Kan, H.: Impact of short-term exposure to fine particulate matter air pollution on urinary metabolome: A randomized, double-blind, crossover trial, Environ. Int., 130, 104878, https://doi.org/10.1016/j.envint.2019.05.072, 2019.

Chen, J., Li, C., Ristovski, Z., Milic, A., Gu, Y., Islam, M. S., Wang, S., Hao, J., Zhang, H., He, C., Guo, H., Fu, H., Miljevic, B., Morawska, L., Thai, P., Lam, Y. F., Pereira, G., Ding, A., Huang, X., and Dumka, U. C.: A review of biomass burning: Emissions and impacts on air quality, health and climate in China, Sci. Total Environ., 579, 1000–1034, https://doi.org/10.1016/j.scitotenv.2016.11.025, 2017.

Chen, S., Xu, L., Zhang, Y., Chen, B., Wang, X., Zhang, X., Zheng, M., Chen, J., Wang, W., Sun, Y., Fu, P., Wang, Z., and Li, W.: Direct observations of organic aerosols in common wintertime hazes in North China: insights into direct emissions from Chinese residential stoves, Atmos. Chem. Phys., 17, 1259–1270, https://doi.org/10.5194/acp-17-1259-2017, 2017.

Chen, W., Tong, D., Zhang, S., Dan, M., Zhang, X., and Zhao, H.: Temporal variability of atmospheric particulate matter and chemical composition during a growing season at an agricultural site in northeastern China, J. Environ. Sci., 38, 133–141, https://doi.org/10.1016/j.jes.2015.05.023, 2015.

Chen, Y., Ebenstein, A., Greenstone, M., and Li, H.: Evidence on the impact of sustained exposure to air pollution on life expectancy from China's Huai River policy, P. Natl. Acad. Sci. USA, 110, 12936–12941, https://doi.org/10.1073/pnas.1300018110, 2013.

Cheng, Y., Engling, G., He, K.-B., Duan, F.-K., Ma, Y.-L., Du, Z.-Y., Liu, J.-M., Zheng, M., and Weber, R. J.: Biomass burning contribution to Beijing aerosol, Atmos. Chem. Phys., 13, 7765–7781, https://doi.org/10.5194/acp-13-7765-2013, 2013.

Cheng, Y., Zheng, G., Wei, C., Mu, Q., Zheng, B., Wang, Z., Gao, M., Zhang, Q., He, K., Carmichael, G., Poschl, U., and Su, H.: Reactive nitrogen chemistry in aerosol water as a source of sulfate during haze events in China, Sci. Adv., 2, e1601530, https://doi.org/10.1126/sciadv.1601530, 2016.

Chi, J. W., Li, W. J., Zhang, D. Z., Zhang, J. C., Lin, Y. T., Shen, X. J., Sun, J. Y., Chen, J. M., Zhang, X. Y., Zhang, Y. M., and Wang, W. X.: Sea salt aerosols as a reactive surface for inorganic and organic acidic gases in the Arctic troposphere, Atmos. Chem. Phys., 15, 11341–11353, https://doi.org/10.5194/acp-15-11341-2015, 2015.

Chowdhury, S., Dey, S., Guttikunda, S., Pillarisetti, A., Smith, K. R., and Di Girolamo, L.: Indian annual ambient air quality standard is achievable by completely mitigating emissions from household sources, P. Natl. Acad. Sci. USA, 116, 10711–10716, https://doi.org/10.1073/pnas.1900888116, 2019.

Cohen, A. J., Brauer, M., Burnett, R., Anderson, H. R., Frostad, J., Estep, K., Balakrishnan, K., Brunekreef, B., Dandona, L., Dandona, R., Feigin, V., Freedman, G., Hubbell, B., Jobling, A., Kan, H., Knibbs, L., Liu, Y., Martin, R., Morawska, L., Pope, C. A., Shin, H., Straif, K., Shaddick, G., Thomas, M., van Dingenen, R., van Donkelaar, A., Vos, T., Murray, C. J. L., and Forouzanfar, M. H.: Estimates and 25-year trends of the global burden of disease attributable to ambient air pollution: an analysis of data from the Global Burden of Diseases Study 2015, Lancet, 389, 1907–1918, https://doi.org/10.1016/s0140-6736(17)30505-6, 2017.

Ding, A. J., Huang, X., Nie, W., Sun, J. N., Kerminen, V. M., Petäjä, T., Su, H., Cheng, Y. F., Yang, X. Q., Wang, M. H., Chi, X. G., Wang, J. P., Virkkula, A., Guo, W. D., Yuan, J., Wang, S. Y., Zhang, R. J., Wu, Y. F., Song, Y., Zhu, T., Zilitinkevich, S., Kulmala, M., and Fu, C. B.: Enhanced haze pollution by black carbon in megacities in China, Geophys. Res. Lett., 43, 2873–2879, https://doi.org/10.1002/2016GL067745, 2016.

Ebenstein, A., Fan, M., Greenstone, M., He, G., and Zhou, M.: New evidence on the impact of sustained exposure to air pollution on life expectancy from China's Huai River Policy, P. Natl. Acad. Sci. USA, 114, 10384–10389, https://doi.org/10.1073/pnas.1616784114, 2017.

Fortems-Cheiney, A., Dufour, G., Hamaoui-Laguel, L., Foret, G., Siour, G., Van Damme, M., Meleux, F., Coheur, P. F., Clerbaux, C., and Clarisse, L.: Unaccounted variability in NH_3 agricultural sources detected by IASI contributing to European spring haze episode, Geophys. Res. Lett., 43, 5475–5482, https://doi.org/10.1002/2016GL069361, 2016.

Frossard, A. A., Shaw, P. M., Russell, L. M., Kroll, J. H., Canagaratna, M. R., Worsnop, D. R., Quinn, P. K., and Bates, T. S.: Springtime Arctic haze contributions of submicron organic particles from European and Asian combustion sources, J. Geophys. Res., 116, D05205, https://doi.org/10.1029/2010JD015178, 2011.

Gao, J., Woodward, A., Vardoulakis, S., Kovats, S., Wilkinson, P., Li, L., Xu, L., Li, J., Yang, J., Li, J., Cao, L., Liu, X., Wu, H., and Liu, Q.: Haze, public health and mitigation measures in China: A review of the current evidence for further policy response, Sci. Total Environ., 578, 148–157, https://doi.org/10.1016/j.scitotenv.2016.10.231, 2017.

Guinot, B., Cachier, H., and Oikonomou, K.: Geochemical perspectives from a new aerosol chemical mass closure, Atmos. Chem. Phys., 7, 1657–1670, https://doi.org/10.5194/acp-7-1657-2007, 2007.

Guo, S., Hu, M., Zamora, M. L., Peng, J., Shang, D., Zheng, J., Du, Z., Wu, Z., Shao, M., Zeng, L., Molina, M. J., and Zhang, R.: Elucidating severe urban haze formation in China, P. Natl. Acad. Sci. USA, 111, 17373–17378, https://doi.org/10.1073/pnas.1419604111, 2014.

Han, S., Wu, J., Zhang, Y., Cai, Z., Feng, Y., Yao, Q., Li, X., Liu, Y., and Zhang, M.: Characteristics and formation mechanism of a winter haze-fog episode in Tianjin, China, Atmos. Environ., 98, 323–330, https://doi.org/10.1016/j.atmosenv.2014.08.078, 2014.

Hand, J. L., Malm, W. C., Laskin, A., Day, D., Lee, T., Wang, C., Carrico, C., Carrillo, J., Cowin, J. P., Collett, J., and Iedema, M. J.: Optical, physical, and chemical properties of tar balls observed during the Yosemite Aerosol Characterization Study, J. Geophys. Res., 110, D21210, https://doi.org/10.1029/2004JD005728, 2005.

He, H., Wang, Y., Ma, Q., Ma, J., Chu, B., Ji, D., Tang, G., Liu, C., Zhang, H., and Hao, J.: Mineral dust and NOx promote the conversion of SO_2 to sulfate in heavy pollution days, Sci. Rep., 4, 4172, https://doi.org/10.1038/srep04172, 2014.

Hoffer, A., Tóth, A., Nyirő-Kósa, I., Pósfai, M., and Gelencsér, A.: Light absorption properties of laboratory-generated tar ball particles, Atmos. Chem. Phys., 16, 239–246, https://doi.org/10.5194/acp-16-239-2016, 2016.

Huang, K., Zhuang, G., Lin, Y., Fu, J. S., Wang, Q., Liu, T., Zhang, R., Jiang, Y., Deng, C., Fu, Q., Hsu, N. C., and Cao, B.: Typical types and formation mechanisms of haze in an Eastern Asia megacity, Shanghai, Atmos. Chem. Phys., 12, 105–124, https://doi.org/10.5194/acp-12-105-2012, 2012.

Huang, R. J., Zhang, Y., Bozzetti, C., Ho, K. F., Cao, J. J., Han, Y., Daellenbach, K. R., Slowik, J. G., Platt, S. M., Canonaco, F., Zotter, P., Wolf, R., Pieber, S. M., Bruns, E. A., Crippa, M., Ciarelli, G., Piazzalunga, A., Schwikowski, M., Abbaszade, G., Schnelle-Kreis, J., Zimmermann, R., An, Z., Szidat, S., Baltensperger, U., El Haddad, I., and Prevot, A. S.: High secondary aerosol contribution to particulate pollution during haze events in China, Nature, 514, 218–222, https://doi.org/10.1038/nature13774, 2014.

Huang, Y., Li, L., Li, J., Wang, X., Chen, H., Chen, J., Yang, X., Gross, D. S., Wang, H., Qiao, L., and Chen, C.: A case study of the highly time-resolved evolution of aerosol chemical and optical properties in urban Shanghai, China, Atmos. Chem. Phys., 13, 3931—3944, https://doi.org/10.5194/acp-13-3931-2013, 2013.

Jung, J., Lee, K., Cayetano, M. G., Batmunkh, T., and Kim, Y. J.: Optical and hygroscopic properties of long-range transported haze plumes observed at Deokjeok Island off the west coast of the Korean Peninsula under the Asian continental outflows, J. Geophys. Res.-Atmos., 120, 8861–8877, https://doi.org/10.1002/2015JD023154, 2015.

Lelieveld, J., Evans, J. S., Fnais, M., Giannadaki, D., and Pozzer, A.: The contribution of outdoor air pollution sources to premature mortality on a global scale, Nature, 525, 367–371, https://doi.org/10.1038/nature15371, 2015.

Li, W. and Shao, L.: Transmission electron microscopy study of aerosol particles from the brown hazes in northern China, J. Geophys. Res., 114, D09302, https://doi.org/10.1029/2008JD011285, 2009.

Li, H., Han, Z., Cheng, T., Du, H., Kong, L., Chen, J., Zhang, R., and Wang, W.: Agricultural Fire Impacts on the Air Quality of Shanghai during Summer Harvesttime, Aerosol Air Qual. Res., 10, 95–101, https://doi.org/10.4209/aaqr.2009.08.0049, 2010.

Li, M., Wang, T., Xie, M., Li, S., Zhuang, B., Huang, X., Chen, P., Zhao, M., and Liu, J.: Formation and Evolution Mechanisms for Two Extreme Haze Episodes in the Yangtze River Delta Region of China During Winter 2016, J. Geophys. Res.-Atmos., 124, 3607–3623, https://doi.org/10.1029/2019JD030535, 2019.

Li, P., Yan, R., Yu, S., Wang, S., Liu, W., and Bao, H.: Reinstate regional transport of $PM_{2.5}$ as a major cause of severe haze in Beijing, P. Natl. Acad. Sci. USA, 112, 2739–2740, https://doi.org/10.1073/pnas.1502596112, 2015.

Li, W., Zhou, S., Wang, X., Xu, Z., Yuan, C., Yu, Y., Zhang, Q., and Wang, W.: Integrated evaluation of aerosols from regional brown hazes over northern China in winter: Concentrations, sources, transformation, and mixing states, J. Geophys. Res., 116, D09301, https://doi.org/10.1029/2010JD015099, 2011.

Li, W., Shi, Z., Zhang, D., Zhang, X., Li, P., Feng, Q., Yuan, Q., and Wang, W.: Haze particles over a coal-burning region in the China Loess Plateau in winter: Three flight missions in December 2010, J. Geophys. Res., 117, D12306, https://doi.org/10.1029/2012JD017720, 2012.

Li, W., Sun, J., Xu, L., Shi, Z., Riemer, N., Sun, Y., Fu, P., Zhang, J., Lin, Y., Wang, X., Shao, L., Chen, J., Zhang, X., Wang, Z., and Wang, W.: A conceptual framework for mixing structures in individual aerosol particles, J. Geophys. Res.-Atmos., 121, 13784–13798, https://doi.org/10.1002/2016JD025252, 2016.

Li, W., Xu, L., Liu, X., Zhang, J., Lin, Y., Yao, X., Gao, H., Zhang, D., Chen, J., and Wang, W.: Air pollution–aerosol interactions produce more bioavailable iron for ocean ecosystems, Sci. Adv., 3, e1601749, https://doi.org/10.1126/sciadv.1601749, 2017.

Li, W. J., Shao, L. Y., and Buseck, P. R.: Haze types in Beijing and the influence of agricultural biomass burning, Atmos.

Chem. Phys., 10, 8119–8130, https://doi.org/10.5194/acp-10-8119-2010, 2010.

Li, X., Ma, Y., Wang, Y., Liu, N., and Hong, Y.: Temporal and spatial analyses of particulate matter (PM_{10} and $PM_{2.5}$) and its relationship with meteorological parameters over an urban city in northeast China, Atmos. Res., 198, 185–193, https://doi.org/10.1016/j.atmosres.2017.08.023, 2017.

Li, X., Song, S., Zhou, W., Hao, J., Worsnop, D. R., and Jiang, J.: Interactions between aerosol organic components and liquid water content during haze episodes in Beijing, Atmos. Chem. Phys., 19, 12163–12174, https://doi.org/10.5194/acp-19-12163-2019, 2019.

Li, Z., Guo, J., Ding, A., Liao, H., Liu, J., Sun, Y., Wang, T., Xue, H., Zhang, H., and Zhu, B.: Aerosol and boundary-layer interactions and impact on air quality, Natl. Sci. Rev., 4, 810–833, https://doi.org/10.1093/nsr/nwx117, 2017.

Lin, M., Biglari, S., Zhang, Z., Crocker, D., Tao, J., Su, B., Liu, L., and Thiemens, M. H.: Vertically uniform formation pathways of tropospheric sulfate aerosols in East China detected from triple stable oxygen and radiogenic sulfur isotopes, Geophys. Res. Lett., 44, 5187–5196, https://doi.org/10.1002/2017GL073637, 2017.

Liu, D., Joshi, R., Wang, J., Yu, C., Allan, J. D., Coe, H., Flynn, M. J., Xie, C., Lee, J., Squires, F., Kotthaus, S., Grimmond, S., Ge, X., Sun, Y., and Fu, P.: Contrasting physical properties of black carbon in urban Beijing between winter and summer, Atmos. Chem. Phys., 19, 6749–6769, https://doi.org/10.5194/acp-19-6749-2019, 2019.

Liu, J., Han, Y., Tang, X., Zhu, J., and Zhu, T.: Estimating adult mortality attributable to $PM_{2.5}$ exposure in China with assimilated $PM_{2.5}$ concentrations based on a ground monitoring network, Sci. Total Environ., 568, 1253–1262, https://doi.org/10.1016/j.scitotenv.2016.05.165, 2016.

Liu, L., Kong, S., Zhang, Y., Wang, Y., Xu, L., Yan, Q., Lingaswamy, A. P., Shi, Z., Lv, S., Niu, H., Shao, L., Hu, M., Zhang, D., Chen, J., Zhang, X., and Li, W.: Morphology, composition, and mixing state of primary particles from combustion sources-crop residue, wood, and solid waste, Sci. Rep., 7, 5047, https://doi.org/10.1038/s41598-017-05357-2, 2017.

Liu, M., Song, Y., Zhou, T., Xu, Z., Yan, C., Zheng, M., Wu, Z., Hu, M., Wu, Y., and Zhu, T.: Fine particle pH during severe haze episodes in northern China, Geophys. Res. Lett., 44, 5213–5221, https://doi.org/10.1002/2017GL073210, 2017.

Liu, Y., Wu, Z., Wang, Y., Xiao, Y., Gu, F., Zheng, J., Tan, T., Shang, D., Wu, Y., Zeng, L., Hu, M., Bateman, A. P., and Martin, S. T.: Submicrometer Particles Are in the Liquid State during Heavy Haze Episodes in the Urban Atmosphere of Beijing, China, Environ. Sci. Technol. Lett., 4, 427–432, https://doi.org/10.1021/acs.estlett.7b00352, 2017.

Ma, L., Li, M., Zhang, H., Li, L., Huang, Z., Gao, W., Chen, D., Fu, Z., Nian, H., Zou, L., Gao, J., Chai, F., and Zhou, Z.: Comparative analysis of chemical composition and sources of aerosol particles in urban Beijing during clear, hazy, and dusty days using single particle aerosol mass spectrometry, J. Clean. Prod., 112, 1319–1329, https://doi.org/10.1016/j.jclepro.2015.04.054, 2016.

Ma, Y., Zhao, H., Dong, Y., Che, H., Li, X., Hong, Y., Li, X., Yang, H., Liu, Y., Wang, Y., Liu, N., and Sun, C.: Comparison of Two Air Pollution Episodes over Northeast China in Winter 2016/17 Using Ground-Based Lidar, J. Meteorol. Res., 32, 313–323, https://doi.org/10.1007/s13351-018-7047-4, 2018.

Mahowald, N. M., Hamilton, D. S., Mackey, K. R. M., Moore, J. K., Baker, A. R., Scanza, R. A., and Zhang, Y.: Aerosol trace metal leaching and impacts on marine microorganisms, Nat. Commun., 9, 2614, https://doi.org/10.1038/s41467-018-04970-7, 2018.

Miao, Y., Guo, J., Liu, S., Zhao, C., Li, X., Zhang, G., Wei, W., and Ma, Y.: Impacts of synoptic condition and planetary boundary layer structure on the trans-boundary aerosol transport from Beijing-Tianjin-Hebei region to northeast China, Atmos. Environ., 181, 1–11, https://doi.org/10.1016/j.atmosenv.2018.03.005, 2018.

Oberdorster, G., Sharp, Z., Atudorei, V., Elder, A., Gelein, R., Kreyling, W., and Cox, C.: Translocation of inhaled ultrafine particles to the brain, Inhal. Toxicol., 16, 437–445, https://doi.org/10.1080/08958370490439597, 2004.

Pósfai, M., Simonics, R., Li, J., Hobbs, P. V., and Buseck, P. R.: Individual aerosol particles from biomass burning in southern Africa: 1. Compositions and size distributions of carbonaceous particles, J. Geophys. Res.-Atmos., 108, D138483, https://doi.org/10.1029/2002jd002291, 2003.

Pósfai, M., Gelencsér, A., Simonics, R., Arató, K., Li, J., Hobbs, P. V., and Buseck, P. R.: Atmospheric tar balls: Particles from biomass and biofuel burning, J. Geophys. Res., 109, D06213, https://doi.org/10.1029/2003JD004169, 2004.

Ren, L., Fu, P., He, Y., Hou, J., Chen, J., Pavuluri, C. M., Sun, Y., and Wang, Z.: Molecular distributions and compound-specific stable carbon isotopic compositions of lipids in wintertime aerosols from Beijing, Sci. Rep., 6, 27481, https://doi.org/10.1038/srep27481, 2016.

Rodo, X., Curcoll, R., Robinson, M., Ballester, J., Burns, J. C., Cayan, D. R., Lipkin, W. I., Williams, B. L., Couto-Rodriguez, M., Nakamura, Y., Uehara, R., Tanimoto, H., and Morgui, J. A.: Tropospheric winds from northeastern China carry the etiologic agent of Kawasaki disease from its source to Japan, P. Natl. Acad. Sci. USA, 111, 7952–7957, https://doi.org/10.1073/pnas.1400380111, 2014.

Sedlacek III, A. J., Buseck, P. R., Adachi, K., Onasch, T. B., Springston, S. R., and Kleinman, L.: Formation and evolution of tar balls from northwestern US wildfires, Atmos. Chem. Phys., 18, 11289–11301, https://doi.org/10.5194/acp-18-11289-2018, 2018.

Shao, J., Chen, Q., Wang, Y., Lu, X., He, P., Sun, Y., Shah, V., Martin, R. V., Philip, S., Song, S., Zhao, Y., Xie, Z., Zhang, L., and Alexander, B.: Heterogeneous sulfate aerosol formation mechanisms during wintertime Chinese haze events: air quality model assessment using observations of sulfate oxygen isotopes in Beijing, Atmos. Chem. Phys., 19, 6107–6123, https://doi.org/10.5194/acp-19-6107-2019, 2019.

Shi, G., Xu, J., Peng, X., Xiao, Z., Chen, K., Tian, Y., Guan, X., Feng, Y., Yu, H., Nenes, A., and Russell, A. G.: pH of Aerosols in a Polluted Atmosphere: Source Contributions to Highly Acidic Aerosol, Environ. Sci. Technol., 51, 4289–4296, https://doi.org/10.1021/acs.est.6b05736, 2017.

Shi, J., Wang, N., Gao, H., Baker, A. R., Yao, X., and Zhang, D.: Phosphorus solubility in aerosol particles related to particle sources and atmospheric acidification in Asian continental outflow, Atmos. Chem. Phys., 19, 847–860, https://doi.org/10.5194/acp-19-847-2019, 2019.

Sobhani, N., Kulkarni, S., and Carmichael, G. R.: Source sector and region contributions to black carbon and $PM_{2.5}$ in the Arctic, Atmos. Chem. Phys., 18, 18123–18148, https://doi.org/10.5194/acp-18-18123-2018, 2018.

Sun, J., Liu, L., Xu, L., Wang, Y., Wu, Z., Hu, M., Shi, Z., Li, Y., Zhang, X., Chen, J., and Li, W.: Key Role of Nitrate in Phase Transitions of Urban Particles: Implications of Important Reactive Surfaces for Secondary Aerosol Formation, J. Geophys. Res.-Atmos., 123, 1234–1243, https://doi.org/10.1002/2017JD027264, 2018.

Sun, Y., Jiang, Q., Wang, Z., Fu, P., Li, J., Yang, T., and Yin, Y.: Investigation of the sources and evolution processes of severe haze pollution in Beijing in January 2013, J. Geophys. Res.-Atmos., 119, 4380–4398, https://doi.org/10.1002/2014JD021641, 2014.

Tao, J., Cao, J.-J., Zhang, R.-J., Zhu, L., Zhang, T., Shi, S., and Chan, C.-Y.: Reconstructed light extinction coefficients using chemical compositions of $PM_{2.5}$ in winter in Urban Guangzhou, China, Adv. Atmos. Sci., 29, 359–368, https://doi.org/10.1007/s00376-011-1045-0, 2012.

Tao, M., Chen, L., Xiong, X., Zhang, M., Ma, P., Tao, J., and Wang, Z.: Formation process of the widespread extreme haze pollution over northern China in January 2013: Implications for regional air quality and climate, Atmos. Environ., 98, 417–425, https://doi.org/10.1016/j.atmosenv.2014.09.026, 2014.

Tian, H. Z., Zhu, C. Y., Gao, J. J., Cheng, K., Hao, J. M., Wang, K., Hua, S. B., Wang, Y., and Zhou, J. R.: Quantitative assessment of atmospheric emissions of toxic heavy metals from anthropogenic sources in China: historical trend, spatial distribution, uncertainties, and control policies, Atmos. Chem. Phys., 15, 10127–10147, https://doi.org/10.5194/acp-15-10127-2015, 2015.

Tie, X., Huang, R. J., Dai, W., Cao, J., Long, X., Su, X., Zhao, S., Wang, Q., and Li, G.: Effect of heavy haze and aerosol pollution on rice and wheat productions in China, Sci. Rep., 6, 29612, https://doi.org/10.1038/srep29612, 2016.

Tóth, A., Hoffer, A., Nyirő-Kósa, I., Pósfai, M., and Gelencsér, A.: Atmospheric tar balls: aged primary droplets from biomass burning?, Atmos. Chem. Phys., 14, 6669–6675, https://doi.org/10.5194/acp-14-6669-2014, 2014.

van Donkelaar, A., Martin, R. V., Brauer, M., Hsu, N. C., Kahn, R. A., Levy, R. C., Lyapustin, A., Sayer, A. M., and Winker, D. M.: Global Estimates of Fine Particulate Matter using a Combined Geophysical-Statistical Method with Information from Satellites, Models, and Monitors, Environ. Sci. Technol., 50, 3762–3772, https://doi.org/10.1021/acs.est.5b05833, 2016.

Wang, G., Zhang, R., Gomez, M. E., Yang, L., Levy Zamora, M., Hu, M., Lin, Y., Peng, J., Guo, S., Meng, J., Li, J., Cheng, C., Hu, T., Ren, Y., Wang, Y., Gao, J., Cao, J., An, Z., Zhou, W., Li, G., Wang, J., Tian, P., Marrero-Ortiz, W., Secrest, J., Du, Z., Zheng, J., Shang, D., Zeng, L., Shao, M., Wang, W., Huang, Y., Wang, Y., Zhu, Y., Li, Y., Hu, J., Pan, B., Cai, L., Cheng, Y., Ji, Y., Zhang, F., Rosenfeld, D., Liss, P. S., Duce, R. A., Kolb, C. E., and Molina, M. J.: Persistent sulfate formation from London Fog to Chinese haze, P. Natl. Acad. Sci. USA, 113, 13630–13635, https://doi.org/10.1073/pnas.1616540113, 2016.

Wang, H., An, J., Shen, L., Zhu, B., Xia, L., Duan, Q., and Zou, J.: Mixing state of ambient aerosols in Nanjing city by single particle mass spectrometry, Atmos. Environ., 132, 123–132, https://doi.org/10.1016/j.atmosenv.2016.02.032, 2016.

Wang, J., Nie, W., Cheng, Y., Shen, Y., Chi, X., Wang, J., Huang, X., Xie, Y., Sun, P., Xu, Z., Qi, X., Su, H., and Ding, A.: Light absorption of brown carbon in eastern China based on 3-year multi-wavelength aerosol optical property observations and an improved absorption Ångström exponent segregation method, Atmos. Chem. Phys., 18, 9061–9074, https://doi.org/10.5194/acp-18-9061-2018, 2018.

Wang, J., Liu, D., Ge, X., Wu, Y., Shen, F., Chen, M., Zhao, J., Xie, C., Wang, Q., Xu, W., Zhang, J., Hu, J., Allan, J., Joshi, R., Fu, P., Coe, H., and Sun, Y.: Characterization of black carbon-containing fine particles in Beijing during wintertime, Atmos. Chem. Phys., 19, 447–458, https://doi.org/10.5194/acp-19-447-2019, 2019.

Wang, Z., Li, J., Wang, Z., Yang, W., Tang, X., Ge, B., Yan, P., Zhu, L., Chen, X., Chen, H., Wand, W., Li, J., Liu, B., Wang, X., Wand, W., Zhao, Y., Lu, N., and Su, D.: Modeling study of regional severe hazes over mid-eastern China in January 2013 and its implications on pollution prevention and control, Sci. China Earth Sci., 57, 3–13, https://doi.org/10.1007/s11430-013-4793-0, 2014.

Wu, Y., Zhang, R., Tian, P., Tao, J., Hsu, S. C., Yan, P., Wang, Q., Cao, J., Zhang, X., and Xia, X.: Effect of ambient humidity on the light absorption amplification of black carbon in Beijing during January 2013, Atmos. Environ., 124, 217–223, https://doi.org/10.1016/j.atmosenv.2015.04.041, 2016.

Wu, Z., Wang, Y., Tan, T., Zhu, Y., Li, M., Shang, D., Wang, H., Lu, K., Guo, S., Zeng, L., and Zhang, Y.: Aerosol Liquid Water Driven by Anthropogenic Inorganic Salts: Implying Its Key Role in Haze Formation over the North China Plain, Environ. Sci. Technol. Lett., 5, 160–166, https://doi.org/10.1021/acs.estlett.8b00021, 2018.

Xie, C., Xu, W., Wang, J., Wang, Q., Liu, D., Tang, G., Chen, P., Du, W., Zhao, J., Zhang, Y., Zhou, W., Han, T., Bian, Q., Li, J., Fu, P., Wang, Z., Ge, X., Allan, J., Coe, H., and Sun, Y.: Vertical characterization of aerosol optical properties and brown carbon in winter in urban Beijing, China, Atmos. Chem. Phys., 19, 165–179, https://doi.org/10.5194/acp-19-165-2019, 2019.

Xing, L., Wu, J., Elser, M., Tong, S., Liu, S., Li, X., Liu, L., Cao, J., Zhou, J., El-Haddad, I., Huang, R., Ge, M., Tie, X., Prévôt, A. S. H., and Li, G.: Wintertime secondary organic aerosol formation in Beijing–Tianjin–Hebei (BTH): contributions of HONO sources and heterogeneous reactions, Atmos. Chem. Phys., 19, 2343–2359, https://doi.org/10.5194/acp-19-2343-2019, 2019.

Xu, L., Liu, L., Zhang, J., Zhang, Y., Ren, Y., Wang, X., and Li, W.: Morphology, Composition, and Mixing State of Individual Aerosol Particles in Northeast China during Wintertime, Atmosphere, 8, 47–57, https://doi.org/10.3390/atmos8030047, 2017.

Xue, J., Yuan, Z., Griffith, S. M., Yu, X., Lau, A. K., and Yu, J. Z.: Sulfate Formation Enhanced by a Cocktail of High NO_x, SO_2, Particulate Matter, and Droplet pH during Haze-Fog Events in Megacities in China: An Observation-Based Modeling Investigation, Environ. Sci. Technol., 50, 7325–7334, https://doi.org/10.1021/acs.est.6b00768, 2016.

Yan, X., Ohara, T., and Akimoto, H.: Bottom-up estimate of biomass burning in mainland China, Atmos. Environ., 40, 5262–5273, https://doi.org/10.1016/j.atmosenv.2006.04.040, 2006.

Yang, T., Gbaguidi, A., Yan, P., Zhang, W., Zhu, L., Yao, X., Wang, Z., and Chen, H.: Model elucidating the sources and formation mechanisms of severe haze pollution over North-

east mega-city cluster in China, Environ. Pollut., 230, 692–700, https://doi.org/10.1016/j.envpol.2017.06.007, 2017.

Yuan, Q., Li, W., Zhou, S., Yang, L., Chi, J., Sui, X., and Wang, W.: Integrated evaluation of aerosols during haze-fog episodes at one regional background site in North China Plain, Atmos. Res., 156, 102–110, https://doi.org/10.1016/j.atmosres.2015.01.002, 2015.

Zhang, J., Liu, L., Wang, Y., Ren, Y., Wang, X., Shi, Z., Zhang, D., Che, H., Zhao, H., Liu, Y., Niu, H., Chen, J., Zhang, X., Lingaswamy, A. P., Wang, Z., and Li, W.: Chemical composition, source, and process of urban aerosols during winter haze formation in Northeast China, Environ. Pollut., 231, 357–366, https://doi.org/10.1016/j.envpol.2017.07.102, 2017.

Zhang, X., Sun, J., Wang, Y., Li, W., Zhang, Q., Wang, W., Quan, J., Cao, G., Wang, J., and Yang, Y.: Factors contributing to haze and fog in China, Chinese Sci. Bull., 58, 1178–1187, https://doi.org/10.1360/972013-150, 2013.

Zhang, Y., Schauer, J. J., Zhang, Y., Zeng, L., Wei, Y., Liu, Y., and Shao, M.: Characteristics of particulate carbon emissions from real-world Chinese coal combustion, Environ. Sci. Technol., 42, 5068–5073, https://doi.org/10.1021/es7022576, 2008.

Zhang, Y., Yuan, Q., Huang, D., Kong, S., Zhang, J., Wang, X., Lu, C., Shi, Z., Zhang, X., and Sun, Y.: Direct observations of fine primary particles from residential coal burning: insights into their morphology, composition, and hygroscopicity, J. Geophys. Res.-Atmos., 123, 12964–12979, https://doi.org/10.1029/2018JD028988, 2018a.

Zhang, Y., Zhang, Q., Cheng, Y., Su, H., Li, H., Li, M., Zhang, X., Ding, A., and He, K.: Amplification of light absorption of black carbon associated with air pollution, Atmos. Chem. Phys., 18, 9879–9896, https://doi.org/10.5194/acp-18-9879-2018, 2018b.

Zhang, Y. L., Kawamura, K., Agrios, K., Lee, M., Salazar, G., and Szidat, S.: Fossil and Nonfossil Sources of Organic and Elemental Carbon Aerosols in the Outflow from Northeast China, Environ. Sci. Technol., 50, 6284–6292, https://doi.org/10.1021/acs.est.6b00351, 2016.

Zhao, B., Zheng, H., Wang, S., Smith, K. R., Lu, X., Aunan, K., Gu, Y., Wang, Y., Ding, D., Xing, J., Fu, X., Yang, X., Liou, K.-N., and Hao, J.: Change in household fuels dominates the decrease in $PM_{2.5}$ exposure and premature mortality in China in 2005–2015, P. Natl. Acad. Sci. USA, 115, 12401–12406, https://doi.org/10.1073/pnas.1812955115, 2018.

Zhao, H., Che, H., Xia, X., Wang, Y., Wang, H., Wang, P., Ma, Y., Yang, H., Liu, Y., Wang, Y., Gui, K., Sun, T., Zheng, Y., and Zhang, X.: Multiyear Ground-Based Measurements of Aerosol Optical Properties and Direct Radiative Effect Over Different Surface Types in Northeastern China, J. Geophys. Res.-Atmos., 123, 13887–13916, https://doi.org/10.1029/2018JD029141, 2018.

Zhao, X. J., Zhao, P. S., Xu, J., Meng,, W., Pu, W. W., Dong, F., He, D., and Shi, Q. F.: Analysis of a winter regional haze event and its formation mechanism in the North China Plain, Atmos. Chem. Phys., 13, 5685–5696, https://doi.org/10.5194/acp-13-5685-2013, 2013.

Zheng, B., Zhang, Q., Zhang, Y., He, K. B., Wang, K., Zheng, G. J., Duan, F. K., Ma, Y. L., and Kimoto, T.: Heterogeneous chemistry: a mechanism missing in current models to explain secondary inorganic aerosol formation during the January 2013 haze episode in North China, Atmos. Chem. Phys., 15, 2031–2049, https://doi.org/10.5194/acp-15-2031-2015, 2015.

Zheng, G. J., Duan, F. K., Su, H., Ma, Y. L., Cheng, Y., Zheng, B., Zhang, Q., Huang, T., Kimoto, T., Chang, D., Pöschl, U., Cheng, Y. F., and He, K. B.: Exploring the severe winter haze in Beijing: the impact of synoptic weather, regional transport and heterogeneous reactions, Atmos. Chem. Phys., 15, 2969–2983, https://doi.org/10.5194/acp-15-2969-2015, 2015.

Zhi, G., Chen, Y., Xue, Z., Meng, F., Cai, J., Sheng, G., and Fu, J.: Comparison of elemental and black carbon measurements during normal and heavy haze periods: implications for research, Environ. Monit. Assess., 186, 6097–6106, https://doi.org/10.1007/s10661-014-3842-2, 2014.

Zhong, J., Zhang, X., Wang, Y., Wang, J., Shen, X., Zhang, H., Wang, T., Xie, Z., Liu, C., Zhang, H., Zhao, T., Sun, J., Fan, S., Gao, Z., Li, Y., and Wang, L.: The two-way feedback mechanism between unfavorable meteorological conditions and cumulative aerosol pollution in various haze regions of China, Atmos. Chem. Phys., 19, 3287–3306, https://doi.org/10.5194/acp-19-3287-2019, 2019.

Zou, J., Wang, M., Zhao, S., Wu, X., Zhao, L., Liu, J., Gao, W., Tang, G., Xin, J., Wang, L., Ji, D., Xu, H., Wang, Y., and Hu, B.: Case study of the effects of aerosol chemical composition and hygroscopicity on the scattering coefficient in summer, Xianghe, southeast of Beijing, China, Atmos. Res., 225, 81–87, https://doi.org/10.1016/j.atmosres.2019.03.026, 2019.